Contents lists available at ScienceDirect

International Journal of Pharmaceutics: X

Development and optimization of vildagliptin solid lipid nanoparticles loaded ocuserts for controlled ocular delivery: A promising approach towards treating diabetic retinopathy

Abd El hakim Ramadan [a], Mahmoud M.A. Elsayed [b,*], Amani Elsayed [c], Marwa A. Fouad [d], Mohamed S. Mohamed [e,f], Sangmin Lee [g,h,**], Reda A. Mahmoud [e,f], Shereen A. Sabry [i], Mohammed M. Ghoneim [j], Ahmed H.E. Hassan [k,l], Reham A. Abd Elkarim [m], Amany Belal [n], Ahmed A. El-Shenawy [e,f]

[a] Department of Pharmaceutics, Faculty of Pharmacy, Port Said University, Port Said 42515, Egypt
[b] Department of Pharmaceutics and Clinical Pharmacy, Faculty of Pharmacy, Sohag University, Sohag 82524, Egypt
[c] Department of Pharmaceutics & Industrial Pharmacy, College of Pharmacy, Taif, University, Taif, Saudi Arabia
[d] Department of Pharmaceutics and Pharmaceutical Technology, Faculty of pharmacy, Deraya University, Minia, Egypt
[e] Department of Pharmaceutics and Pharmaceutical Technology, Faculty of Pharmacy, Al-Azhar University, Assiut Branch, Assiut 71524, Egypt
[f] Al-Azhar Centre of Nano Sciences and Applications, Al-Azhar University, Assiut, Egypt
[g] Department of Fundamental Pharmaceutical Science, Graduate School, Kyung Hee University, 26 Kyungheedae-ro, Dongdaemun-gu, Seoul 02447, Republic of Korea
[h] Department of Regulatory Science, Graduated School, Kyung Hee University, 26 Kyungheedae-ro, Dongdaemun-gu, Seoul 02447, Republic of Korea
[i] Department of Pharmaceutics, Faculty of Pharmacy, Zagazig University, Zagazig 44519, Egypt
[j] Department of Pharmacy Practice, College of Pharmacy, AlMaarefa University, Ad Diriyah, 13713, Saudi Arabia
[k] Department of Medicinal Chemistry, Faculty of Pharmacy, Mansoura University, Mansoura 35516, Egypt
[l] Medicinal Chemistry Laboratory, College of Pharmacy, Kyung Hee University, 26 Kyungheedae-ro, Seoul 02447, Republic of Korea
[m] Ministry of Health and Population, Assiut, Egypt
[n] Department of Pharmaceutical Chemistry, College of Pharmacy, Taif University, P.O. Box 11099, Taif 21944, Saudi Arabia

ARTICLE INFO

ABSTRACT

Diabetes mellitus (DM) is the most prevalent cause of diabetic retinopathy (DRP). DRP has been recognized for a long time as a microvascular disease. Many drugs were used to treat DRP, including vildagliptin (VLD). In addition to its hypoglycemic effect, VLD minimizes ocular inflammation and improves retinal blood flow for individuals with type 2 diabetes mellitus. Nevertheless, VLD can cause upper respiratory tract infections, diarrhea, nausea, hypoglycemia, and poor tolerability when taken orally regularly due to its high water solubility and permeability. Effective ocular administration of VLD is achieved using solid lipid nanoparticles (SLNPs), which improve corneal absorption, prolonged retention, and extended drug release. Ocuserts (OCUs) are sterile, long-acting ocular dosage forms that diminish the need for frequent dosing while improving residence time and stability. Therefore, this study intends to develop VLD solid lipid nanoparticle OCUs (VLD-SLNPs-OCUs) to circumvent the issues commonly associated with VLD. SLNPs were prepared using the double-emulsion/melt dispersion technique. The optimal formula has been implemented in OCUs. Optimization and development of VLD-SLNPs-OCUs were performed using a Box-Behnken Design (BBD). VLD-SLNPs-OCUs loading efficiency was $95.28 \pm 2.87\%$, and differential scanning calorimetry data (DSC) showed the full transformation of VLD to an amorphous state and the excellent distribution in the prepared OCUs matrices. The *in vivo* release of VLD from the optimized OCUs after 24 h was $35.12 \pm 2.47\%$, consistent with *in vitro* drug release data of 36.89 ± 3.11. The optimized OCUs are safe to use in the eye, as shown by the ocular irritation test. VLD-SLNPs-OCUs provide extended VLD release, an advantageous alternative to conventional oral dose forms, resulting in fewer systemic adverse effects and less variation in plasma drug levels. VLD-SLNPs-OCUs might benefit retinal microvascular

* Corresponding author at: Department of Pharmaceutics and Clinical Pharmacy, Faculty of Pharmacy, Sohag University, Sohag 82524, Egypt.
** Corresponding author at: Department of Fundamental Pharmaceutical Science, Graduate School, Kyung Hee University, 26 Kyungheedae-ro, Dongdaemun-gu, Seoul 02447, Republic of Korea.
E-mail addresses: mahmoudalmenshawy@pharm.sohag.edu.eg (M.M.A. Elsayed), leesm@khu.ac.kr (S. Lee).

blood flow beyond blood glucose control and may be considered a promising approach to treating diabetic retinopathy.

1. Introduction

Diabetes Mellitus (DM) is a long-term condition that develops when the pancreas does not create enough insulin or the body cannot properly utilize the insulin it produces (Balaji et al., 2019). Diabetic retinopathy (DRP) is a progressive dysfunction of the retinal blood vessels due to chronic hyperglycemia. DRP may be a complication of type 1 or type 2 DM (Mbata et al., 2017). At first, it is asymptomatic, but if not treated, it can cause vision loss or blindness (Dekhil et al., 2019). There are currently over 285 million DM sufferers, which is projected to go up to 439 million by 2030. DRP accounts for 1.8 million of the world's total blindness (37 million) (Balaji et al., 2019). Duration of DM and severity of hyperglycemia are the major risk factors for DRP (Leske et al., 2005). The main treatment of DRP includes laser treatment, eye injections with anti-VEGF such as ranibizumab and aflibercept, steroid eye implants, and eye surgery (vitreoretinal surgery) (Mansour et al., 2020). These treatments have side effects such as bleeding and developing a small blind spot close to the center of vision, as with laser treatment (Porta and Bandello, 2002); blood clots may be formed, which lead to heart attack or stroke, as with eye injections (Costagliola et al., 2012); increased pressure inside the eye and cataracts as with a steroid implant (Stewart, 2012); developing further bleeding into the eye; retinal detachment; and infection in the eye as with surgery (Repka et al., 2006). Suppose a drug or drug delivery system that can improve retinal microvascular blood flow and bypass the side effects mentioned above effect is considered a trend in ophthalmic drug delivery systems. Pancreatic islet stimulation by vildagliptin (VLD) enhances the glucose sensitivity of pancreatic α and β cells by selectively inhibiting the 4 dipeptidyl-peptidase (DPP-4) enzyme. VLD reduces hepatic glucose synthesis and therefore, lowers plasma glucose levels by raising the insulin: glucagon ratio (Wu et al., 2015). In addition to lowering blood glucose levels, recent studies have shown that VLD can reduce ocular inflammation and increase retinal blood flow in patients with type 2 diabetes mellitus, suggesting that VLD may have additional, beneficial effects on retinal microvascular blood flow and thus be considered a promising approach to treating vision

disorders (Berndt-Zipfel et al., 2013; Nandi et al., 2022). The Biopharmaceutics Classification System (BCS) classifies VLD as class I, among other highly water-soluble, highly permeable drugs. Conventional oral dosage forms of VLD offer little control over drug administration, which results in large variations in plasma drug levels, which is one of the major downsides of utilizing VLD due to its short elimination half-life (1.4–2.3 h) (Garrison et al., 2015). Long-term use is associated with an increased risk of otitis media, diarrhea, nausea, hypoglycemia, and intolerability. In 2022, Nandi, et al., studied the possible ocular anti-inflammatory effect of VLD using a topically applied plasticized ocular film formulation (Nandi et al., 2022). They prepared the ocular films by solvent cast and evaporation technique utilizing triethanolamine, dimethyl sulphoxide, and polyethylene glycol 400 (PEG 400) as plasticizers in hydroxypropyl methylcellulose (HPMC) hydrogel matrix base. They studied the VLD anti-inflammatory actions in the carrageenan-induced ocular rabbit model. They concluded that the hydration degree, film swelling, and erosion rate of the prepared film were the main controlling factors in the process of VLD release, ocular residence time, and drug permeation. Solid lipid nanoparticles (SLNPs) offer a way to achieve therapeutic benefits with a lower dosage and fewer systemic adverse effects. As an alternative to conventional colloidal carrier systems, SLNPs are constructed out of solid lipids that are tolerated by the body physiology and then dispersed in an aqueous surfactant solution with a typical diameter of 100–150 nm. The advantages of SLNPs include their high stability, low toxicity to the body, high drug-loading capacity with little drug leakage, drug targeting, and controlled and/or prolonged drug release (Jampilek and Kralova, 2020). They are lipophilic and tiny; therefore, they can easily cross biological barriers. SLNPs are an effective ocular drug delivery technology due to their mucoadhesive characteristics, sterilization tolerance, increased corneal absorption, prolonged ocular retention time, and sustained drug release profile without compromising visual acuity (Akhter et al., 2022). The development of SLNPs as carriers for water-soluble compounds has proven challenging, despite their use as a delivery system for lipophilic medicines (Paul et al., 2022). The ability to accurately deliver an
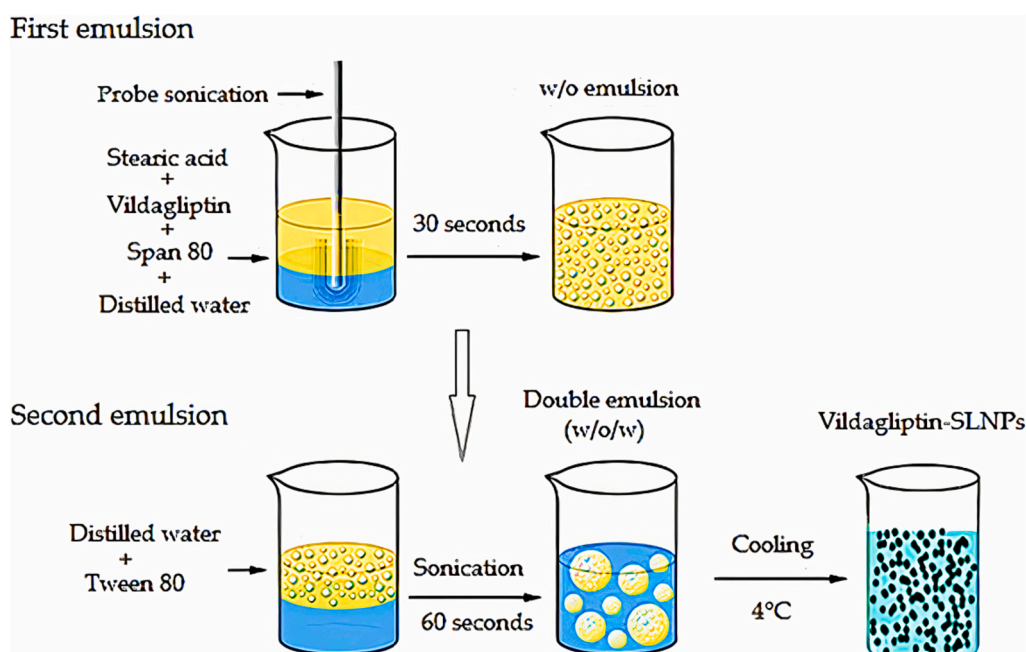
Fig. 1. Schematic depiction of procedures that comprise the preparation of VLD-SLNPs.

Table 1
Composition of various VLD-SLNPs formulations.

Component	Run 1	Run 2	Run 3	Run 4	Run 5	Run 6	Run 7	Run 8
VLD (mg)	50	50	50	50	50	50	50	50
Stearic acid (gm)	0.5	0.5	0.5	0.5	1	1	1	1
Span 80 (mL)	2.5	2.5	5	5	2.5	2.5	5	5
Tween 80 (mL)	2.5	5	2.5	5	2.5	5	2.5	5
Distilled water to (mL)	20	20	20	20	20	20	20	20

ophthalmic drug delivery system without causing blurred vision or eye irritation, having an appropriate mucoadhesive time to improve drug retention in the pre-corneal area and thereby increase drug bioavailability, having limited systemic absorption through nasolacrimal drainage, and reducing the need for frequent dosing regimens leading to improved outcomes are generally the main requirements for an ideal ophthalmic drug delivery system. Ocuserts (OCUs) are drug delivery systems that may be solid or semisolid, usually prepared from polymeric materials, designed to be inserted in the conjunctival sac to deliver the loaded drug to the ocular tissues. The main insert benefits are precise drug dosing, increased ocular residence time, reduced systemic side effects, and better patient compliance (Shivhare et al., 2012). OCUs could be utilized to overcome the problems of traditional ophthalmic preparations, facilitating more efficient therapy (Rahić et al., 2020). This is, as far as we are aware, the first attempt to prepare an SLNPs-loaded OCUs formulation of VLD with the basic objective of increasing drug pre-corneal residence time, prolonged release time, reducing the frequency of drug administrations, and thus improving patient compliance and therapeutic efficacy. Besides lowering the blood glucose level, we focus on the utility of using VLD to improve retinal blood flow. Which makes them a promising approach to treating diabetic retinopathy and bypassing the side effects associated with the traditional treatment.

2. Materials and Methods

2.1. Materials

Vildagliptin (VLD) was a gift sample from EVA Pharm Company, Cairo, Egypt. Stearic acid, Span 80, Tween 80, soy lecithin, glyceryl monostearate (GMS), polyvinyl alcohol (PVA), acetone, acetonitrile (HPLC grade), and beeswax were purchased from Sigma Chemical Co., Saint Louis, Missouri, USA. Hydroxypropyl methylcellulose (HPMC), propylene glycol (PG), ethyl alcohol, and methanol (analytical grade) were purchased from El-Nasr Pharmaceutical Company, Cairo, Egypt. Eudragit RL100 was supplied by Fluka Chemika, Buchs, Switzerland. The rest of the chemicals were of analytical grade and were utilized as they were without further purification.

2.2. Methodology

2.2.1. Preformulation investigations

Analysis of VLD by UV spectroscopy, study of the compatibility between the drug and excipient using Fourier transform infrared spectroscopy (FTIR), and lipid screening *via* solubility study are shown in the supplementary materials file.

2.2.2. Preparation of vildagliptin-solid lipid nanoparticles

Vildagliptin solid-lipid nanoparticles (VLD-SLNPs) were fabricated utilizing stearic acid (as the lipid), Tween 80 (as the water-soluble surfactant), and Span 80 (as the lipid surfactant) employing a double-emulsion/melt-dispersion approach (Fig. 1). The drug: lipid ratio was 1:10 and 1:20. Briefly, accurate weights of stearic acid were heated to 75 ± 1 °C (above its melting temperature) and mixed with the accurately weighed amounts of VLD and Span 80 (lipid-soluble surfactant) under magnetic stirring (MSH-ORO, USA). Hot distilled water (75 ± 1 °C) (2

mL) was added, and the mixture was sonicated using an ultrasonic processor, GE130, probe CV18, Australia; for 30 s. at 50% amplitude (20 W) to form the first emulsion (w/o). The first emulsion was warmed to the desired temperature (75 ± 1 °C), and then the appropriate volume of a warm Tween 80 aqueous solution (75 ± 1 °C) was added. The mixture was then homogenized by ultrasonic vibrations at 50% amplitude (20 W) in pulse cycles (10 s; on, 5 s; off) for 60 s, generating the double emulsion (w/o/w). The obtained double emulsion was gently added to 60 mL of cold distilled water (4 ± 1 °C) under magnetic stirring at 1500 rpm for 15 min to stabilize the obtained SLNPs and promote their solidification (Peres et al., 2016). The amounts of components used in the Preparation of each VLD-SLNP formulation are mentioned in (Table 1).

2.2.3. Characterization of the prepared VLD-SLNPs

2.2.3.1. Percentage yield (% yield) estimation.
The % yield was estimated from the weight of the dried VLD-SLNPs recovered from each formulation and the sum of the initial dry weight of the materials utilized in its formulation (Eq. 1) (Rampino et al., 2013).

$$\%\text{yield} = \frac{\text{Weight of the recovered SLNPs}}{\text{The initial weight of VLD and excipients}} \times 100 \quad (1)$$

2.2.3.2. Particle size and polydispersity index (PDI).
The particle size and PDI of the developed VLD–SLNP dispersions were evaluated by the dynamic light scattering method *via* a Zeta sizer device (Malvern Nano ZS, Germany). After appropriate dilution with distilled water (1: 60), sample particle size (by intensity) and PDI were investigated. All the experiments were determined in triplicates, and the data were reported as the average value ± standard deviation (SD). The measurement angle was equal to 90° and the refractive index of the SLNPs and distilled water were set at 1.35 and 1.33, respectively and the temperature was 25 ± 0.5 °C (El-Shenawy et al., 2020; Elsayed et al., 2021).

2.2.3.3. Zeta potential determination.
VLD-SLNP zeta potentials were determined using Zeta Sizer Nano ZS (ZEN 3600) (Malvern Instruments; Malvern, United Kingdom). Each sample was adequately diluted with distilled water (1:60). The zeta potential of the samples was determined by photon correlation spectroscopy. The samples were placed in a transparent disposable cell with a temperature of 25 ± 0.5 °C. All measurements were repeated in three times and the results were presented as mean values ± SD (Mohamed et al., 2019; Sabry et al., 2021).

2.2.3.4. Quantification of VLD.
The reversed-phase high-performance liquid chromatography (RP-HPLC) technique, HPLC standard curve, validation for accuracy and precision, the limit of detection (LOD), and the limit of quantification (LOQ) are shown in the supplementary materials file.

2.2.3.5. Entrapment efficiency.
Entrapment efficiency (EE) indicates the percent of VLD entrapped in the fabricated SLNPs. The EE of the investigated VLD-SLNPs was determined by an indirect method in which VLD-SLNPs were separated from the aqueous medium containing unentrapped VLD by ultracentrifugation at 16000 rpm for 30 min at 4 °C using a cooling ultracentrifuge (Bioevopeak, CFGR-B580, Shandong, China). The HPLC method was used to determine free VLD in the

supernatant λ_{max} 212 nm. Eq. 2 was used to calculate the EE. All measurements were retested three times and the values obtained were expressed as mean $\pm$ SD (El-Shenawy et al., 2021; Auda et al., 2010; Hesham et al., 2015; Refaat et al., 2019).

$$EE\ (\%) = \frac{\text{The total amount of VLD} - \text{Unentrapped VLD}}{\text{The total amount of VLD}} \times 100 \quad (2)$$

2.2.3.6. Total drug content (TDC). Total VLD quantity in various fabricated VLD–SLNPs formulations was investigated by adding 1 mL of the dispersion in 9 mL of acetone and phosphate buffer, pH 7.4 (1:1 *v/v*), and the mixture was sonicated for 30 min to extract VLD completely (ultrasonic cleaner set, WUG-D06H, Korea). Afterward, we filtered the samples with 0.2 μm filters and determined the concentration of VLD using a UV spectrophotometer (UV–visible spectrophotometer model UV-1800, Shimadzu, Japan) at λ_{max} of 212 nm (Elsayed et al., 2021; Gao et al., 2021). TDC was calculated using eq. 3.

$$TDC = \text{VLD concentration} \times \text{dilution factor} \times \text{volume of the formulation} \quad (3)$$

2.2.3.7. In vitro dissolution studies. *In vitro* dissolution studies were conducted for pure VLD, and the formulated VLD–SLNPs formulations *via* dialysis bag method using a dialysis membrane with a molecular weight cutoff of 12,000 Da, Sigma Chem. Co. (USA). We washed the dialysis membrane with distilled water before use, and then soaked it for 24 h in the dissolution medium (phosphate buffer, pH 7.4). VLD-SLNPs various formulations dispersion equivalent to 20 mg VLD (based on TDC of the formulations) were dispersed in an equivalent volume of the dissolution medium and charged into a dialysis bag with the two ends carefully tied by clamps and immersed in the dissolution cell of the dissolution tester apparatus, SR II, 6 flasks (paddle type), Hanson Research Co., USA, containing 500 mL of the dissolution medium at 100 $\pm$ 1 rpm and 37 $\pm$ 0.5 °C. At the predetermined time intervals (0.5, 1, 2, 3, 4, 6, 8, 10, 12, 16, 18, and 24 h), 5 mL was removed from the cell and restored with an equal volume of new dissolving media to keep the sink condition constant. The various samples were analyzed spectrophotometrically at λ_{max} of 212 nm. All experiments were performed in triplicate against a blank (Abd Elkarim et al., 2022; Elsayed et al., 2020a).

2.2.3.8. Morphological studies. To investigate the surface morphology of the selected SLNPs, VLD-SLNPs dispersion, Run 3 was subjected to scanning electron microscopy (SEM) studies (Elsayed et al., 2020b; Elsayed et al., 2019). A droplet of the chosen SLNPs dispersion was placed on a transparent glass stub, dried by air, and coated with a sputter coater of polaron (E5100). The droplet was visualized under SEM (SMM-5400 LV–SEM) (Jeol, Japan) and photographed. The SEM was operating at 15.0 KV (Abdelhameed et al., 2022; El-Shenawy et al., 2023).

2.2.4. Selection of VLD-SLNPs for incorporation in OCUs

VLD-SLNPs were chosen for insertion into OCUs based on their tiny particle size, high EE, and low cumulative % release after 24 h, in descending ranking order.

2.2.5. VLD-SLNPs loaded OCUs (VLD-SLNPs-OCUs): Construction and characteristics

2.2.5.1. Preparation of VLD-SLNPs-OCUs. A Box-Behnken design was developed utilizing Stat point Tech., Inc., Warrenton, VA, USA (Stratigraphic Plus® 18 software), (Elsayed et al., 2022a). Each independent variable at three values was used to optimize the formulated VLD-SLPs-OCUs formulations (Elkot et al., 2019; Elsayed, 2021; Elsayed et al., 2020a; Elsayed et al., 2022a; Elsayed et al., 2022b; Solanki et al., 2007). The HPMC concentration (R_1) chosen values were 20 (−1), 40 (0), and 60 (+1) mg, whereas the selected values for PVA (R_2) were 20 (−1), 40 (0), and 60 (+1) mg, and Eudragit RL100 concentration (R_3) were 50

Table 2
VLD-SLNPs-OCUs different formulations composition according to Box Behnken design.

F. Code	VLD–SLNPs (#: Equivalent to)	Drug reservoir			Rate controlling membrane	
		HPMC (mg)	PVA (mg)	PG (mL)	Eudragit RL100 (mg)	PG (mL)
VSO-1	#705 mg VLD	20	20	0.25	100	0.5
VSO-2	#705 mg VLD	60	20	0.25	100	0.5
VSO-3	#705 mg VLD	20	60	0.25	100	0.5
VSO-4	#705 mg VLD	60	60	0.25	100	0.5
VSO-5	#705 mg VLD	20	40	0.25	50	0.5
VSO-6	#705 mg VLD	60	40	0.25	50	0.5
VSO-7	#705 mg VLD	20	40	0.25	150	0.5
VSO-8	#705 mg VLD	60	40	0.25	150	0.5
VSO-9	#705 mg VLD	40	20	0.25	50	0.5
VSO-10	#705 mg VLD	40	60	0.25	50	0.5
VSO-11	#705 mg VLD	40	20	0.25	150	0.5
VSO-12	#705 mg VLD	40	60	0.25	150	0.5
VSO-13	#705 mg VLD	40	40	0.25	100	0.5
VSO-14	#705 mg VLD	40	40	0.25	100	0.5
VSO-15	#705 mg VLD	40	40	0.25	100	0.5

(−1), 100 (0), 150 (−1) mg (Table 2). *Ex vivo* mucoadhesive time (MAT) (Z_1) and cumulative % released after 24 h (Z_2) were chosen as dependent variables.

2.2.5.2. Preparation of the drug reservoir films. The accurately weighed amounts (Table 2) of polymers were dissolved in distilled water while heating for 2 h at 60 $\pm$ 1 °C with continuous stirring in a water bath (MSH–ORO, USA). The weighed amount of VLD–SLPNs, Run 3 was added to the previous solution. The final volume was adjusted to 20 mL with distilled water and the stirring was continued for 1 h at 24 $\pm$ 1 °C., the resultant mixture was placed in a Petri dish when mixing was completed (diameter equal to 12 cm) and then placed in the hot air oven for 24 h at 40 $\pm$ 1 °C. A glass funnel was inverted above the Petri dish to ensure the slow and uniform evaporation of the solvent during heating (Shanmugam et al., 2016). A stainless-steel borer was used to cut the film after drying into circular pieces of definite size (10 mm in diameter) containing 25 mg of VLD.

2.2.5.3. Preparation of rate-controlling membrane (RCM). A precise quantity (Table 2) of ingredient (Eudragit RL100) and propylene glycol (PG) as a plasticizer was dissolved in methanol/ distilled water (1:9 *v/v*) (The final volume was adjusted to 20 mL) at room temperature with constant and continuous stirring for 60 min. The formed dispersion was cast for 24 h at 25 $\pm$ 1 °C in a Petri dish with a diameter of 12 cm. A glass funnel was inverted and placed on top of the Petri dish to control the rate and pattern of solvent evaporation (Abdul Ahad et al., 2011). After complete drying, the films were cut into uniformly sized circles (10 mm in diameter) using a borer made from stainless steel.

2.2.5.4. Sealing of the fabricated films. The drug reservoir was sandwiched between two RCMs of the same size (10 mm diameter). Sealing was performed by chloroform application on the edges of the RCM to obtain VLD–SLNPs–OCUs. VLD-SLNPs-OCUs were stored in airtight, amber-colored glass bottles until further investigations (Ahad et al., 2021).

2.2.5.5. Physical evaluation of VLD-SLNPs-OCUs
2.2.5.5.1. Uniformity of weight and thickness. Five OCUs from each

batch were arbitrarily chosen and weighed separately using a digital balance (Radwag, Poland). The average weight of the OCUs was measured. The thickness of the fabricated OCUs was measured at five different points of each investigated OCU formulation using a micrometer screw gauge ($n = 3$) (Nagpal et al., 2020).

2.2.5.5.2. Surface pH measurement. The OCUs were soaked in a Petri dish containing 10 mL distilled water for 30 min. The electrodes of a digital pH sensor (JENWAY 3310, UK) were positioned on the surface of the OCU under investigation, and the system was allowed to equilibrate for one minute. After that, the pH levels were recorded (n = 3) (Dawaba and Dawaba, 2019).

2.2.5.5.3. Folding endurance (FE). The film's FE was assessed by repeatedly folding it at the same point until it showed no signs of breaking. The value of FE (n = 3) was stated as the number of times the OCU could be folded in half without breaking (Takeuchi et al., 2020).

2.2.5.5.4. Drug loading. Each of the OCUs under examination had its total encapsulated VLD quantified by dissolving the investigated OCUs samples first in methanol/ phosphate buffer, pH 7.4 (1:9 *v/v*), and the VLD amount was calculated utilizing eq. 4 obtained for the VLD standard curve.

$$y = 0.0351x - 0.01 \qquad (4)$$

Where y = UV-absorbance and x = VLD concentration (µg/mL). The total encapsulated VLD was compared with the total VLD amount added during the OCUs formulation to determine the approximate drug loading of the investigated OCUs (Naguib et al., 2021).

2.2.5.5.5. Percent moisture absorption (% MA). A percent moisture absorption test was performed to check the physical integrity of the prepared VLD-SLNPs-OCUs in conditions of high humidity. The selected VLD–SLNPs-OCUs from each batch were initially weighed (W0) and placed in a desiccator containing 100 mL of aluminum chloride saturated solution, and $75 \pm 5\%$ humidity was maintained. The OCU samples were taken out after 3 days and reweighed (WF) (Nithiyananthan et al., 2009). The % MA was calculated according to Eq. (5).

$$\%MA = \frac{WF - W0}{W0} \times 100 \qquad (5)$$

2.2.5.5.6. Percent moisture loss (% ML). A percent moisture loss test was carried out to check the integrity of the VLD–SLNPs-OCUs formulations when kept in dry conditions. The VLD-SLNPs-OCUs formulations were initially weighed (W0) and kept in desiccators containing anhydrous calcium chloride. After three days, the investigated VLD-SLNPs-OCUs samples were withdrawn and reweighed individually (WF) (Reddy, 2017). The % ML was estimated according to eq. 6.

$$\%ML = \frac{W0 - WF}{W0} \times 100 \qquad (6)$$

2.2.5.5.7. Swelling index (% swelling). The swelling of the OCUs depends on the concentration of the used polymer, its ionic strength, and the presence of water. To determine the % swelling of formulated VLD-SLNPs-OCUs, Three OCUs from each formula were weighed separately (WD) and each OCU was placed in a beaker containing 5 mL of freshly prepared phosphate buffer, pH 7.4 at 32 ± 0.5 °C. At the specified time interval, 60 min (up to 2 h), the investigated OCU was removed, the surface buffer was removed utilizing filter paper, and the ocusert was reweighed (WS) and then the OCUs returned back to the same beaker. The weighing of the investigated OCUs at the predetermined time intervals was continued until there is no further increase in weight (Tofighia et al., 2017). The % swelling was calculated according to Eq. (7).

$$\%swelling = \frac{WS - WD}{WD} \times 100 \qquad (7)$$

2.2.5.5.8. Ex vivo mucoadhesion time. The formulated VLD-SLNPs-OCUs formulations were subjected to an *ex vivo* mucoadhesion time (MAT) test. The MAT was investigated (in triplicate) after the application of VLD-SLNPs-OCUs formulations (10 mm diameter) on a freshly

Table 3
Sterility test specifications.

Media I	Fluid thioglycolate	
Media II	Soybean–casein digest	
Incubation period	14 days	
Incubation temperature	Media I	30–35 °C
	Media II	20–25 °C

cut sheep eyelid. The animal eyelid, with a length of 2.8 cm, was glued to the bottom of a glass beaker (500 mL). The investigated VLD-SLNPs-OCUs formula (wetted from one side by 100 µL phosphate buffer, pH 7.4) was attached to the mucosal surface of the eyelid by applying a light force with a fingertip for one minute. The beaker was filled with 250 mL of phosphate buffer, pH 7.4 maintained at 37 ± 1 °C, and stirred at a rate of 100 rpm. The time necessary for complete erosion or detachment of the OCUs from the mucosal surface was recorded and considered as MAT (residence time), and the obtained data were expressed as the mean $\pm$ SD (Ramkanth et al., 2009).

2.2.5.6. In vitro release studies and their kinetics. Since the *in vitro* release of drugs from the OCUs has no reported official method, a simple technique was used to evaluate the VLD *in vitro* release patterns from the prepared OCUs. Briefly, in 10 mL phosphate buffer, pH 7.4 contained in 20 mL glass vials the investigated formulations were added. A thermostatically controlled shaking water bath (Kotterman La-bortechnik GmBh, Germany) was used to keep the vials at 37 ± 0.5 °C and 50 strokes/min. Samples of the release media (1 mL) were taken at regular intervals for 24 h, filtered, and diluted with phosphate buffer, pH 7.4. Samples were analyzed spectrophotometrically to quantify VLD concentrations at λ_{max} of 212 nm. The withdrawn samples were replaced with the same volumes of phosphate buffer, pH 7.4. *In vitro*, release experiments were repeated three times and expressed as cumulative VLD percentage released against time. Zero-order (cumulative % of the VLD released *vs.* time), first-order (log cumulative % of the VLD remaining *vs.* time), and Higuchi-diffusion (cumulative % of the VLD released *vs.* square root of time) equations were used to determine the mechanism of VLD release from the fabricated VLD-SLNPs-OCUs formulations (Elsayed et al., 2022b).

2.2.5.7. Differential scanning calorimetry (DSC) analysis. The thermal behavior of the pure VLD, lyophilized VLD-SLNPs, HPMC, PVA, stearic acid, Eudragit RL100, and the lyophilized optimized VLD-SLNPs-OCUs formulation (VSO-0) was investigated using differential scanning calorimetry (DSC60, Shimadzu; Kyoto, Japan) (Ahmed, 2017; Ahmed, 2019; Ahmed et al., 2013). Samples were precisely weighed into aluminum pans and sealed. All samples were run at a heating rate of 10 °C/min over a temperature range of 25–300 °C under an atmosphere of nitrogen, and the DSC thermograms were recorded (El-Shenawy et al., 2023; Hasan et al., 2020).

2.2.5.8. Sterilization of the VSO-0. Sterilization of VSO-0 formulae was performed by placing the formulations under ultraviolet light (each side of the OCUs was exposed for 30 min). The space between the OCUs and the UV lamp was ~30 cm. The sterilized OCUs were stored in sterilized aluminum foil until further investigations (sterility test and *in vivo* release studies) (Senthil Kumar et al., 2017).

2.2.5.9. Sterility test. Sterility evaluation is a very important parameter in the OCU's quality control tests. When conducting the sterility test, many scientists followed the recommendations of the Indian Pharmacopoeia and used the direct inoculation method. 2 mL of VSO-0 solution was taken out using a sterile needle and then added aseptically to various media (Baranowski et al., 2014). The test conditions are presented in Table 3.

2.2.5.10. In vivo release studies. The main drawback of conventional ophthalmic dosage forms is rapid clearance from the eye surface. Novel ophthalmic delivery systems, such as OCUs, are being fabricated to overcome the short precorneal residence time. Out of 15 batches of VLD-SLNPs-OCUs formulations, the optimized formulation, VSO-0, was selected for *in vivo* release studies. The VSO-0 was sterilized by UV radiation for 1 h before the beginning of the study procedures. New-Zealand Albino rabbits of either sex, weighing between 2.1 and 2.7 Kg ($n = 24$, every 3 rabbits were considered as one group, 8 groups), were utilized for the *in vivo* release assessment. The rabbits were housed in individual cages and customized to laboratory conditions for three days of free access to food and potable water with dark/ light regular cycles. The VSO-0 OCUs (10 mm diameter) were placed into the lower conjunctival *cul-de-sac* of the right eye of each animal. The VSO-0 OCUs were inserted into each of the rabbits' right eyes, and the left eye of the rabbits served as control. The 8 groups (each consisting of 3 rabbits) received the OCUs at the same time. The inserted OCUs were carefully removed at 1 h (group 1), 2 h (group 2), 4 h (group 3), 8 h (group 4), 12 h (group 5), 16 h (group 6), 20 h (group 7) and 24 h (group 8), and analyzed spectrophotometrically for drug content as mentioned in the drug loading section at λ_{max} of 212 nm. The remaining VLD amount in the tested removed ocusert was subtracted from the initial drug content of VSO-0 to obtain the amount of VLD released in the rabbit eye (Abdul Ahad et al., 2011). After each experiment, the animals used were sent to the animal house for disposal according to its rules. The procedure was approved by the Ethical Committee No (ZA-AS/PH/19/C/2023). All the experiments followed the 3R's principles (the basic) and The ARRIVE Essential 10.

2.2.5.11. Rabbit ocular irritation test. The evaluation of potential ocular irritation effects of VSO-0 on the cornea or conjunctiva of adult albino rabbits (body weight = 2.4 ± 0.2 Kg, $n = 5$) was evaluated by the Draize eye irritancy test. The eye irritancy potential of VSO-0 was determined by its ability to cause injury to the animal eye's cornea, iris, and conjunctiva when it is applied to the eye. The tested OCUs (10 mm diameter) were placed in the *cul-de-sac* of the left eye, whereas the right eye was considered the control. Visual observation is performed every 2 h until the assigned VSO-0 has completely dissolved to determine the level of irritation. At regular intervals for 7 days after instillation, the degree of inflammation in the anterior portion of the eye was graded based on the presence or absence of symptoms (such as redness, increased tear production, ulceration, eyelid swelling, and iritis) (Nair et al., 2018). The score system assessed the corneal opacity (scored from 0 to 4), iritis (from 0 to 2), and conjunctival redness (from 0 to 3). The ultimate score was calculated by summing the cornea, iris, and conjunctiva scores, which extend from 0 to 9. The score criteria were characterized according to the following cutoffs: under 1: non-irritating; 1 to 4: mildly irritating; 5 to 7: moderately irritating; over 7: severely irritating.

2.2.5.12. Speeded-up experiments on stability. The stability study of the optimized VSO-0 formula was studied using accelerated stability experiments under ICH recommendations. VSO-0 was stored at 40 ± 1 °C/ $75 \pm 3\%$ relative humidity conditions for 6 months (long-term stability study). At predetermined time intervals (1, 2, 3, 4, and 6 months), VSO-0 samples were withdrawn and evaluated for physical appearance, drug loading, and cumulative % VLD amount released at 24 h and compared to the same parameters obtained for the freshly prepared VSO-0 (Nair et al., 2018).

2.2.6. Statistical analysis

The significance of the results was performed by one-way analysis of variance (ANOVA) using SPSS version 23. Result variations were considered statistically significant at $p < 0.05$. All the results values were represented as the mean values $\pm$ SD ($n = 3$) (Kerkhof et al., 2010).

Table 4
% yield, PS, PDI, ZP, EE, TDC, and cumulative % dissolved at 24 h of various VLD–SLNPs formulations.

Formulae	% yield	PS (nm)	PDI	ZP (mV)	EE (%)	TDC (mg)	*Cum.* % at 24 h
Run1	56.83 ± 2.51	189.6 ± 2.05	0.402 ± 0.03	−17.6 ± 1.56	35.32 ± 1.09	4.89 ± 0.491	61.87 ± 3.67
Run2	60.52 ± 4.78	142.2 ± 1.14	0.167 ± 0.01	−15.4 ± 2.67	38.20 ± 1.25	4.35 ± 0.423	69.31 ± 2.98
Run3	64.02 ± 2.33	137.8 ± 2.43	0.256 ± 0.10	−18.1 ± 1.60	43.44 ± 3.17	4.71 ± 0.375	57.04 ± 4.02
Run4	69.51 ± 1.96	122.4 ± 1.09	0.120 ± 0.07	−19.7 ± 1.25	57.21 ± 1.32	4.57 ± 0.233	64.55 ± 2.55
Run5	72.63 ± 2.05	281.9 ± 4.50	0.426 ± 0.03	−21.9 ± 2.33	18.84 ± 2.62	4.81 ± 0.520	37.89 ± 4.16
Run6	89.73 ± 4.21	247 ± 2.43	0.292 ± 0.11	−22.8 ± 2.09	20.42 ± 2.33	4.44 ± 0.472	51.23 ± 3.54
Run7	81.5 ± 3.19	258 ± 2.05	0.373 ± 0.05	−21.3 ± 1.12	22.35 ± 1.48	4.75 ± 0.557	27.63 ± 2.68
Run8	79.58 ± 2.64	202 ± 3.19	0.241 ± 0.04	−23.2 ± 1.48	26.26 ± 2.45	4.07 ± 0.368	43.75 ± 3.15

PS: particle size, PDI: polydispersity index, ZP: zeta potential, EE: entrapment efficiency, TDC: total drug content, and *cum*: cumulative.

3. Results and discussion

3.1. Preformulation studies

VLD spectrophotometric standard curve, spectrum, and lipid screening are shown in (Figs. S1, S2, and S3). The utilized analysis method accuracy and precision were listed in Table S1 and S2 (supplementary materials file).

3.1.1. Drug-excipients compatibility study: infrared spectroscopies using the Fourier transform (FTIR)

FTIR spectra of VLD (Fig. S4) showed principal peaks found at 3293.71 cm^{-1} corresponding to NH (stretching vibration), 2850.07 cm^{-1} corresponding to alkane CH (stretching), prominent peak at 2237.96 cm^{-1} corresponding to nitrile (C≡N) (stretching vibration). Also, VLD showed peaks at 1656.14, 1454.14, and 1225.35 cm^{-1}, corresponding to amide C═O, N═O, and C—N (stretching), respectively. The obtained peaks were similar to the literature peaks confirming the purity of VLD (Shrestha et al., 2014). The FTIR spectrum of HPMC exhibited a characteristic peak at 3455.16 cm^{-1} corresponding to O—H (stretching) and at 1378.98 cm^{-1} due to -OH (bending vibration) (Iqbal et al., 2017). The FTIR spectrum of PVA showed major peaks for hydroxyl and acetate groups at 3425.15 cm^{-1}. The C—H from the alkyl group (stretching) at 2919.92 cm^{-1} and peaks at 1735.61 and 1647.29 cm^{-1} due to C═O and C—O (stretching) were also recorded (Iqbal et al., 2017). For the Eudragit RL100 FTIR spectrum, firm peaks were obtained at 1148.22 and 1243.38 cm^{-1} because of carbonyl ester group stretching vibrations of Eudragit RL100. Absorbance peaks at 1734.27 and 3436.41 cm^{-1} revealed the presence of C═O (ester) and associated -OH groups, respectively (Sharma et al., 2011). The C—H stretching peaks of PG were observed at 1378.05 and 1458.99 cm^{-1} with an absorption band at 2933.21 cm^{-1} belonging to stretching of -COH. FTIR spectra of pure stearic acid showed absorption peaks at 2917.66 and 2849.30 cm^{-1}, which were attributed to -CH$_2$- (asymmetric and symmetric stretching vibration), respectively. Stearic acid FTIR spectra also peaked at 1702 cm^{-1}, belonging to the –COOH group (Zhu et al., 2016). The

FTIR spectrum of Tween 80 showed asymmetric and symmetric stretching peaks at 2924.20 and 2857.58 cm^{-1} for the -CH$_2$ group, respectively, and a stretching peak at 1735.97 cm^{-1} due to the C═O ester group, and a broad peak at 3423.83 cm^{-1} owing of the -OH group's stretching vibration. Span 80 exhibited characteristic FTIR peaks at 3006.28, 2925.26, and 1711.72 cm^{-1} due to aliphatic -OH stretching, C—H stretching, and C═O ester stretching, respectively (Roy Choudhury et al., 2013). The FTIR spectrum of the physical mixture of VLD with excipients utilized for SLNPs and OCU formulations showed the characteristic peaks of VLD. It could be concluded that no new chemical bonds were formed between the VLD and other excipients because the spectra showed no evidence of any new bands, so these excipients can be used effectively fabricating SLNPs and OCUs formulation (El-Emam et al., 2020).

3.2. Characterization of the prepared VLD-SLNPs

3.2.1. Percentage yield, particle size, PDI, and zeta potential

The % yield of the investigated various formulations ranged between $56.83 \pm 2.51\%$ (Run1) and $89.73 \pm 4.21\%$ (Run 6), as shown in Table 4. Nanoparticles (NPs) with a diameter of <200 nm are preferred for ocular drug administration because of their greater capacity to penetrate across corneal barriers (Sahoo et al., 2008). Here, the particle size of VLD-SLNPs ranged from 122.4 ± 1.09 nm to 281.9 nm, and PDI was between 0.120 and 0.426, as shown in Table 4 and Fig. S5a. Run 4 batch showed the smallest particle size, 122.4 ± 1.09 nm, which may be attributed to the lowest lipid and highest surfactant concentrations. Increasing lipid concentration increases NP size ($p < 0.05$), which can be explained by the tendency of lipids to coalesce at high concentrations (Emami et al., 2015). Moreover, particle size decreases while increasing the surfactant concentration as it stabilizes the formed emulsion by a thick protective layer preventing its aggregation *via* the reduction of interfacial tension (Langevin et al., 2004). PDI values were low for the SLNPs formulated with lower lipids and higher surfactant concentrations. This criterion may be because, at a higher surfactant concentration the interfacial tension decreases; thus, the size of the droplet decreases, and the degree of homogeneity increases. PDI values below 0.5 indicate monodispersity (Spoorthy et al., 2023) (Table 4).

Zeta potential is an electric potential created by a charge on the nanoparticle surface. It indicates the degree of repulsion between similarly charged nanoparticles in the prepared SLNP formulation and hence the physical stability (Mehrad et al., 2018). Nanoparticle stabilization is best achieved at values below -30 mV. Due to the hydrolysis of stearic acid, the formed VLD-SLNPs are negatively charged with free fatty acids (Chauhan and Singh, 2023). The zeta potential values ranged from -23.2 ± 1.48 mV to -15.4 ± 2.67 mV (Table 4). Run 3 has zeta potential with a value of -18.1 ± 1.60 mV, as appeared in Fig. S5b. Despite our formulations having a lower zeta potential value, we predict their stability because of the coat formed by Tween 80. The obtained stabilization is the sum of greater steric stabilization and minor electrostatic stabilization. The surface coverage of SLNPs reduces the electrophoretic mobility of the particles, thereby decreasing the zeta potential (Seyfoddin et al., 2010).

3.2.2. Quantification of VLD

HPLC standard curve, accuracy, precision, LOD, and LOQ are shown in (Tables S3 and S4 and Figs. S6 and S7, supplementary materials file).

3.2.3. Entrapment efficiency (EE)

The EE of the prepared VLD-SLNP formulations varied from 18.84 ± 2.62 (Run 5) to $57.21 \pm 1.32\%$ (Run 4), as shown in Table 4. The obtained results showed a slight decrease in EE while increasing the lipid concentration, which may be attributed to the hydrophilicity of VLD and hydrophobicity of the lipid ($p < 0.05$). On the other hand, increasing surfactant concentration increases EE due to the formation of micelles, which entrap more VLD. Also, the higher surfactant concentration
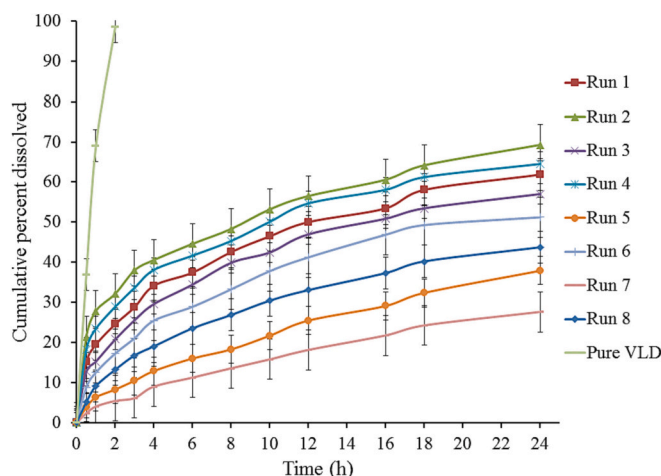
Fig. 2. The comparative dissolution profiles of VLD-SLNPs formulations and pure VLD in phosphate buffer, pH 7.4.
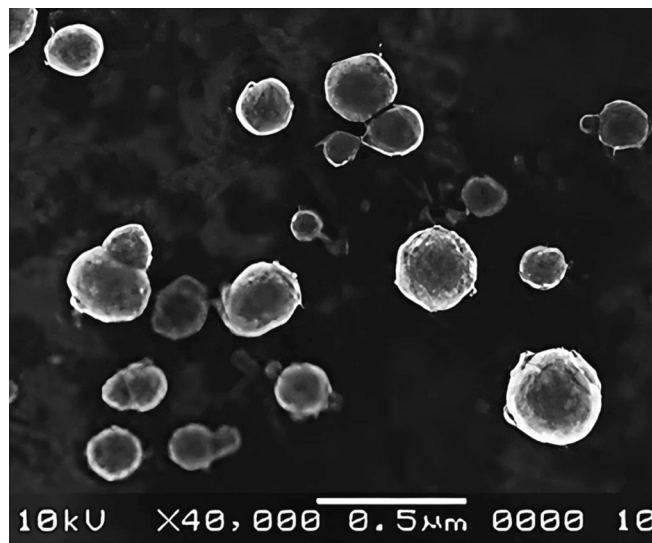
Fig. 3. The SEM imaging of VLD-SLNPs formulation, Run 3.

increases the solubilization of VLD in the lipid phase and consequently increases EE (Subedi et al., 2009).

3.2.4. In vitro VLD-SLNPs dissolution studies

The *in vitro* dissolution profiles of VLD-SLNP formulations compared to pure VLD at 24 h are illustrated in Fig. 2. The dissolution profiles showed a biphasic dissolution pattern characterized by a rapid initial burst followed by a sustained dissolution period. The rapid initial burst could be attributed to VLD molecules attached to the external shell and on the NP's surface, while the sustained pattern can be explained by VLD encapsulation in the SLNP core (Abo-Zeid et al., 2022). The cumulative percent dissolved at 24 h ranged from $27.63 \pm 2.68\%$ (Run 7) to $69.31 \pm 2.98\%$ (Run 2), depending on the variation of the lipid and surfactant concentrations. The high lipid concentration increases the viscosity of the solidified NPs, which would also retard the VLD diffusion to the dissolution medium (Manjunath et al., 2005). The results also revealed that as the concentration of Tween 80 (With higher HLB, 15) increased, the cumulative percent VLD amount increased. The SLNPs formulations with Tween 80 showed faster dissolution behavior than those with Span 80 (HLB of Span 80 = 4.3) (p < 0.05) since the higher HLB value of surfactant facilitates the drug dissolution from the SLNPs (Permana et al., 2019).

Table 5
Evaluation parameters of prepared VLD-SLNPs-OCUs formulations.

F. Code	Weight (mg)	Thickness (mm)	pH	FE	Drug loading (%)
VSO-1	28.65 ± 0.491	0.45 ± 0.04	6.91 ± 0.23	74 ± 1.98	97.12 ± 1.06
VSO-2	29.28 ± 0.473	0.52 ± 0.02	7.02 ± 0.15	80 ± 3.51	94.89 ± 2.99
VSO-3	29.19 ± 0.612	0.49 ± 0.02	7.15 ± 0.10	98 ± 1.06	95.40 ± 3.12
VSO-4	30.87 ± 0.459	0.66 ± 0.02	7.13 ± 0.29	100 ± 2.74	91.78 ± 2.39
VSO-5	28.92 ± 0.388	0.47 ± 0.02	7.24 ± 0.12	84 ± 2.06	94.57 ± 1.33
VSO-6	29.54 ± 0.401	0.57 ± 0.03	6.72 ± 0.26	85 ± 2.90	91.65 ± 2.36
VSO-7	30.22 ± 0.487	0.59 ± 0.03	6.85 ± 0.27	94 ± 3.12	88.15 ± 1.15
VSO-8	31.56 ± 0.522	0.68 ± 0.07	7.37 ± 0.15	95 ± 1.33	93.20 ± 2.54
VSO-9	28.54 ± 0.666	0.42 ± 0.05	6.88 ± 0.23	69 ± 1.64	90.11 ± 2.85
VSO-10	30.36 ± 0.389	0.64 ± 0.08	7.23 ± 0.45	96 ± 1.27	96.33 ± 2.17
VSO-11	30.34 ± 0.602	0.60 ± 0.02	6.90 ± 0.17	81 ± 2.21	90.58 ± 2.04
VSO-12	31.84 ± 0.443	0.76 ± 0.04	7.34 ± 0.19	105 ± 1.33	97.72 ± 2.54
VSO-13	28.86 ± 0.341	0.47 ± 0.05	6.99 ± 0.12	92 ± 3.96	89.64 ± 3.01
VSO-14	28.74 ± 0.355	0.46 ± 0.04	6.85 ± 0.26	90 ± 1.67	95.14 ± 1.08
VSO-15	28.93 ± 0.497	0.49 ± 0.03	6.82 ± 0.17	89 ± 1.14	93.56 ± 1.11

3.2.5. Selection of SLNPs for incorporation in OCUs

According to ranking order, Run 3 was selected for the formulation of OCUs based on the lowest particle size, higher EE, and lowest cumulative % dissolved after 24 h.

3.2.6. Morphological studies

Run 3 morphological studies by SEM are illustrated in Fig. 3. The majority of the VLD-SLNPs were demonstrated to be round, with a flat top and a low degree of polydispersity.

3.3. Physical evaluation of VLD-SLNPs-OCUs

3.3.1. Uniformity of weight and thickness

The average weights of OCUs were found to be in the range of 28.54 ± 0.666 mg (VSO-9) to 31.84 ± 0.443 mg (VSO-12), as listed in Table 5, indicating a uniform distribution of constituents, during the casting of the formulations in the Petri dish could be the main reason for the narrow range of OCUs weight. If the distribution of the dispersion constituents was varied between different film areas the weight variation would increase (Colter, 2016). The average thickness of OCUs was between 0.42 ± 0.05 mm (VSO-9) and 0.76 ± 0.04 mm (VSO-12), as listed in Table 5; this slight variation may be due to the different amounts of polymer used in OCUs preparation (Dawaba et al., 2018).

3.3.2. Surface pH measurement

The surface pH ranged between 6.72 ± 0.26 (VSO-6) and 7.37 ± 0.15 (VSO-8), as shown in Table 5, which approximates the pH of the lacrimal fluid (Hind and Goyan, 1949). Thus, it could be assumed that the OCUs will not induce irritation upon insertion into the eye.

3.3.3. Folding endurance (FE)

FE ranged from 105 ± 1.33 (VSO-12) to 69 ± 1.64 (VSO-9), as shown in Table 5. The marked difference in FE is the function of using various polymers and concentrations. OCUs containing higher concentrations of PVA acquired maximum FE, which may be due to their continuous polymeric structure, which cannot be broken easily (Rao et al., 2018).

3.3.4. Drug loading

Drug loading ranged from 88.15 ± 1.15 (VSO-7) to 97.72 ± 2.54% (VSO-12) (Table 5). This result may be attributed to the amount of HPMC and PVA in the drug reservoir. Increasing the concentration of the polymer increases the drug's encapsulation.

3.3.5. Percentage MA and % ML

The data demonstrated that % MA ranged between 1.38 ± 0.172% (VSO-11) and 6.55 ± 0.344% (VSO-5), as illustrated in Fig. 4, revealing that lower concentrations of Eudragit RL100 (hydrophobic polymer with negligible water absorption ability) resulted in higher % MA values with no change in the OCUs integrity ($p < 0.05$) (Kulhari et al., 2011). The % ML ranges between 10.56 ± 0.324% (VSO-5) and 3.12 ± 0.145% (VSO-12). The minimum % ML was mainly due to the higher concentrations of Eudragit RL100 (RCM), which retain the moisture within the matrix as shown by the formulations VSO-7, 8, 11, and 12 (Thakur et al., 2014).

3.3.6. Swelling index (% swelling)

All the investigated OCUs showed relatively accepted swelling index and the recorded swelling index after the time required for the
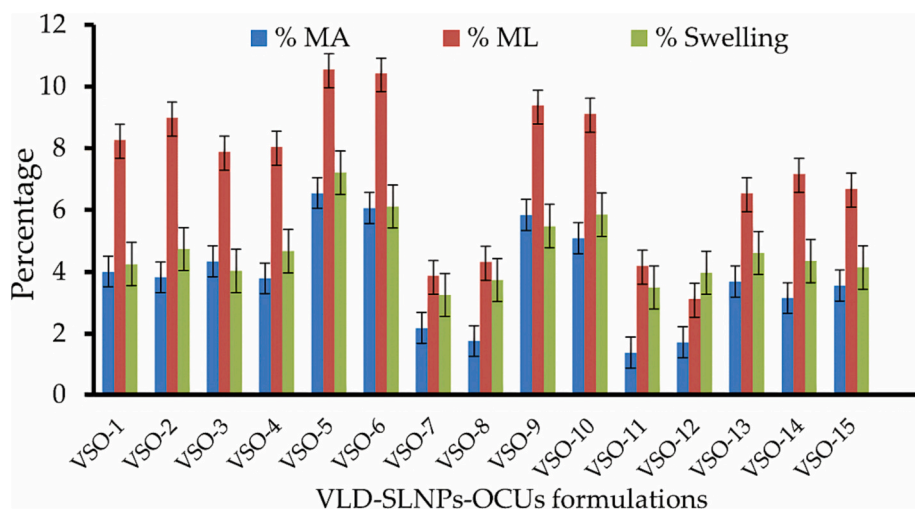
Fig. 4. Percentage of moisture absorption, moisture loss, and swelling index of various vildagliptin-solid lipid nanoparticles loaded ocuserts formulations.
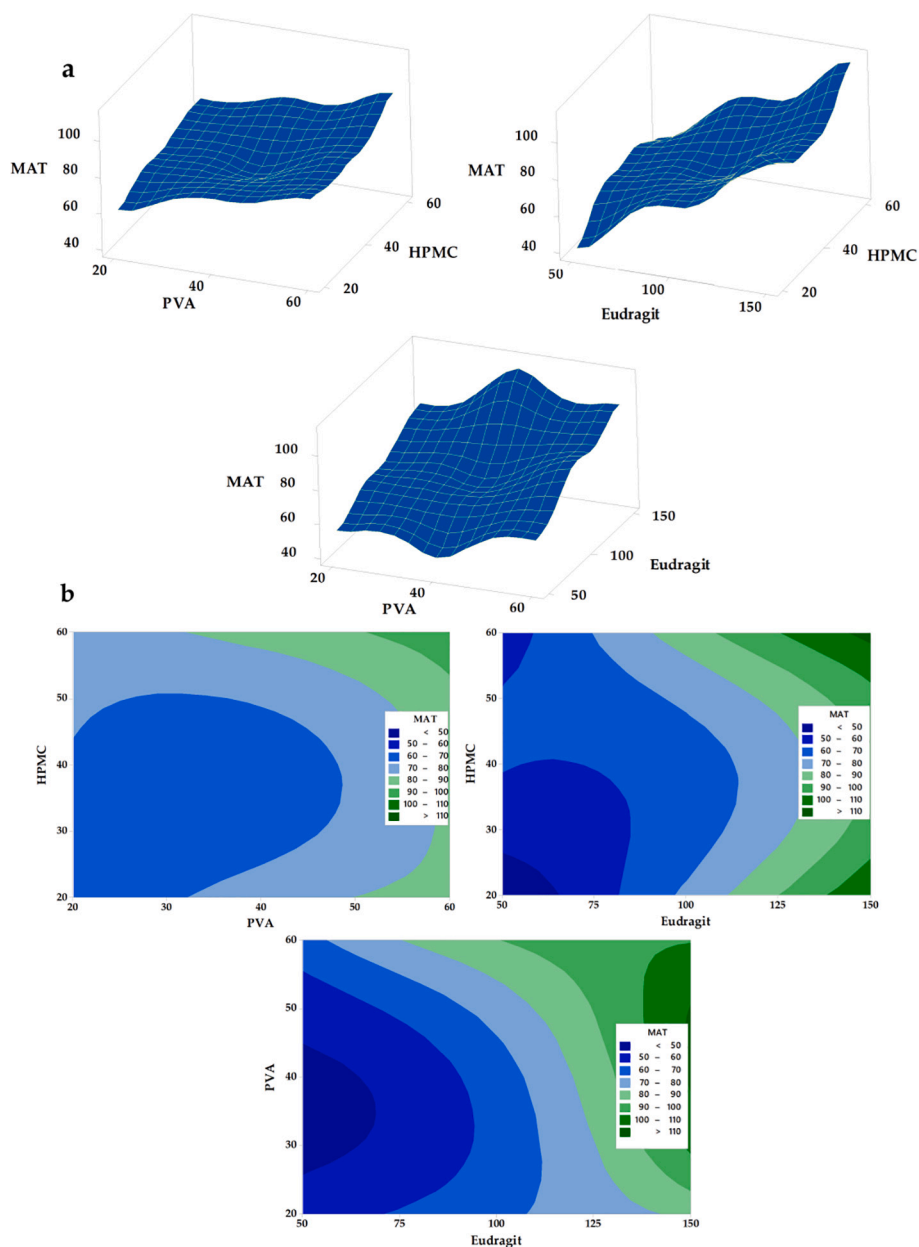
Fig. 5. (a) 3D and response surface plots for the effect of HPMC, PVA, and Eudragit RL100 (R_1, R_2, and R_3) on MAT (Z_1), (b) The contour plot for the effect of HPMC, PVA, and Eudragit RL100 (R1, R2, and R3) on MAT (Z1).

equilibrium (2 h) were illustrated in Fig. 4. The data showed that the percentage swelling of the investigated OCUs ranged between 3.2 ± 0.473% (VSO-7) and 7.21 ± 0.633% (VSO-5) which is considered insignificant ($p > 0.05$). Thus, it could be assumed that the prepared VLD-SLNPs-OCUs would not cause discomfort like a foreign body in the eye. There was no evidence of erosion caused by the expansion of OCUs during the swelling study, and the formulations had excellent cohesive qualities that kept the OCUs functioning as a hydrated adhesive layer for an extended time. This will ensure that the OCUs stay on the eye's surface and continue to emit VLD throughout time (Aburahma and Mahmoud, 2011). This small swelling index is attributed to the presence of quaternary ammonium groups in the Eudragit RL100 structure (Rathod et al., 2017).

3.4. Optimization of VLD-SLNPs-OCUs

The main objective of the optimization process is to increase MAT

and extend the VLD release to enhance its ocular bioavailability. To achieve that, we apply statistical analysis and study the visual contour plots and response surface figures to get the efficient levels of the dependent variables.

3.4.1. Ex vivo mucoadhesion time (MAT)

The data showed that Eudragit RL100 concentration significantly affects MAT, unlike HPMC concentration, which doesn't affect MAT ($p < 0.05$). Also, PVA concentration does not significantly affect MAT ($p > 0.05$), as exhibited by the response and contour plots (Figs. 5, and S8, S9). The lines in contour plots are separated and markedly changed in color from dark blue (MAT <50 min) to dark green color (MAT >110 min) with the increase of Eudragit RL 100 concentration. The increased MAT with a high Eudragit RL100 concentration may be due to the electrostatic interaction between the polymer and the mucosal layer (Boddupalli et al., 2010). HPMC and PVA have low mucoadhesive properties; this is noticeable in the difference in MAT from the low to the
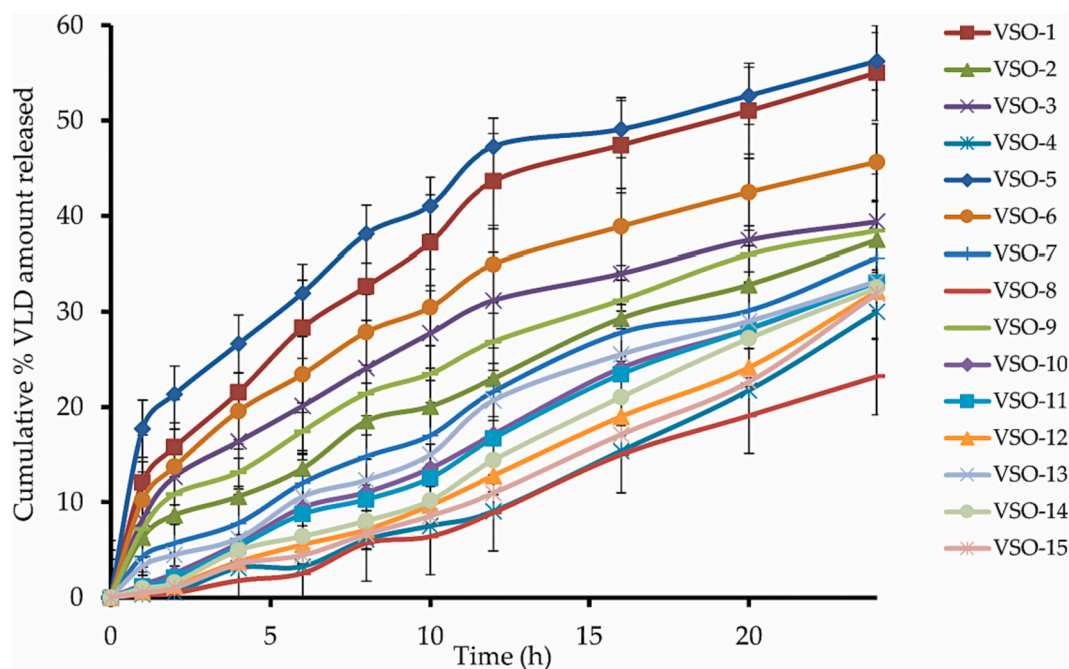
Fig. 6. *In vitro* release profiles of various VLD-SLNPs-OCUs in phosphate buffer, pH 7.4.

high level of the two variables. The contour plots showed a few graded lines from light blue (MAT = 60–70 min) to light green colors (MAT = 80–90 min), confirming HPMC and PVA's nonsignificant effect on MAT ($p > 0.05$). The nonsignificant effect of HPMC and PVA may be due to their double coats (dual-sides) with Eudragit RL100 in a rate-controlling membrane, which is assumed to erode first; thus, the effect of HPMC and PVA is nonsignificant. The results revealed a proportional relationship between MAT and the Eudragit RL100 concentration (Eq. 8, Fig. S9), indicating that Eudragit RL100 possesses non-neglectable mucoadhesive properties and its role as a film-forming polymer. The obtained results with Nandi et al., 2022 showed that the maximum swelling rate was 363 h^{-1} and the film containing dimethyl sulphoxide exhibited the highest *in vitro* release as well as *ex vivo* rabbit ocular permeation. The authors concluded that the investigated film formulation has shown a fast recovery of rabbit ocular inflammation when compared to the untreated rabbit eye after inducing inflammation (Nandi et al., 2022).

The optimization output suggests the optimized formula of MAT consists of 60 mg HPMC, 60 mg PVA, and 150 mg Eudragit RL100.

$$MAT = 57.7 - 1.13\ R_1 - 0.57\ R_2 + 0.071\ R_3 + 0.0215\ R_1{}^2 + 0.0121\ R_2{}^2$$
$$+ 0.00221\ R_3{}^2 - 0.0019\ R_1 R_2 - 0.00244\ R_1 R_3 + 0.00136\ R_2 R_3 \tag{8}$$

3.4.2. In vitro release studies and their kinetics

It concluded from the results that increasing the concentrations of HPMC and Eudragit RL100 had a statistically significant decrease ($p < 0.05$) in the *in vitro* release of VLD from the ocuserts after 24 h, whereas increasing PVA concentration insignificantly decreased ($p > 0.05$) the VLD release rate, as shown in Figs. 6, and 7. The response and contour plots confirmed these results. The lines in contour plots are separated and markedly changed in color from dark green (Rel 24 h > 55%) to dark blue color (Rel 24 h < 25%) with the increase of Eudragit RL 100 and HPMC concentration. This decrease in the amount of VLD released may be due to the increased hydrophobicity of ocuserts and a reduction in their solubility, providing a controlled release rate of VLD (Shafie and Rady, 2012). Although HPMC is a hydrophilic polymer with a low molecular weight and is assumed to have a higher release rate due to ease of water permeation, increasing its concentration significantly decreases VLD release ($p < 0.05$), which may be due to its high swelling behavior, which allows the inclusion of water within the polymer matrix which

opposes drug release (Dawaba et al., 2018). In the case of PVA, during its formulation as a film, it is plasticized by PG, which causes cross-linking of PVA, which hinders VLD release (Kodavaty and Deshpande, 2014).

The present work shows that the main objective is to increase the drug residence time and slow the VLD release rate to improve VLD bioavailability. That objective was achieved by the dual coating of the drug reservoir by Eudragit RL100 in a rat-controlling membrane (RCM). This RCM slows eroding, reducing VLD release in addition to HPMC in the inner core, which controls the VLD release rate (El-Rasoul and Ahmed, 2010; El-Shenawy et al., 2023). Eq. (9) shows a significant correlation between HPMC and Eudragit concentrations and VLD release (Fig. S10).

$$Rel\ 24\ h = 110 - 1.864\ R_1 - 0.994\ R_2 + 0.205\ R_3$$
$$+ 0.0174\ R_{12} + 0.00249\ R_{22}$$
$$+ 0.00028\ R_{32} - 0.00507\ R_1 R_2 - 0.00045\ R_1 R_3 + 0.00109\ R_2 R_3 \tag{9}$$

According to the optimization result, the optimum composition of VLD-SLNPs-OCUs is 50.3 mg HPMC, 60 mg PVA, and 150 mg Eudragit RL100.

The result showed that the cumulative % release after 24 h ranged between $23.21 \pm 2.18\%$ (VSO-8) and $56.23 \pm 3.63\%$ (VSO-5). The increase in PG (plasticizer) in both the drug reservoir (above 1.25% v/v) and RCM (above 2.5%) did not significantly affect the *in vitro* release of VLD, as shown from trial experiments ($p > 0.05$). PG interposes between every individual strand of the used polymer, and the breakdown of the polymer-polymer bonds results in converting the OCUs into a flexible, highly porous, and less cohesive structure (Dawaba and Dawaba, 2019). When the *in vitro* release data were plotted according to the Zero-order equation, VLD-SLNPs-OCUs showed good linearity with higher correlation than First-order and Higuchi–Diffusion models, Indicating Zero-order release model for all VLD-SLNPs-OCUs formulations as shown in Table S5 (supplementary materials file).

3.5. Preparation and characterization of the optimized VLD-SLNPs-OCUs formula (VSO-0)

The optimized VSO-0 OCUs (composed of 50.303 mg HPMC, 60 mg
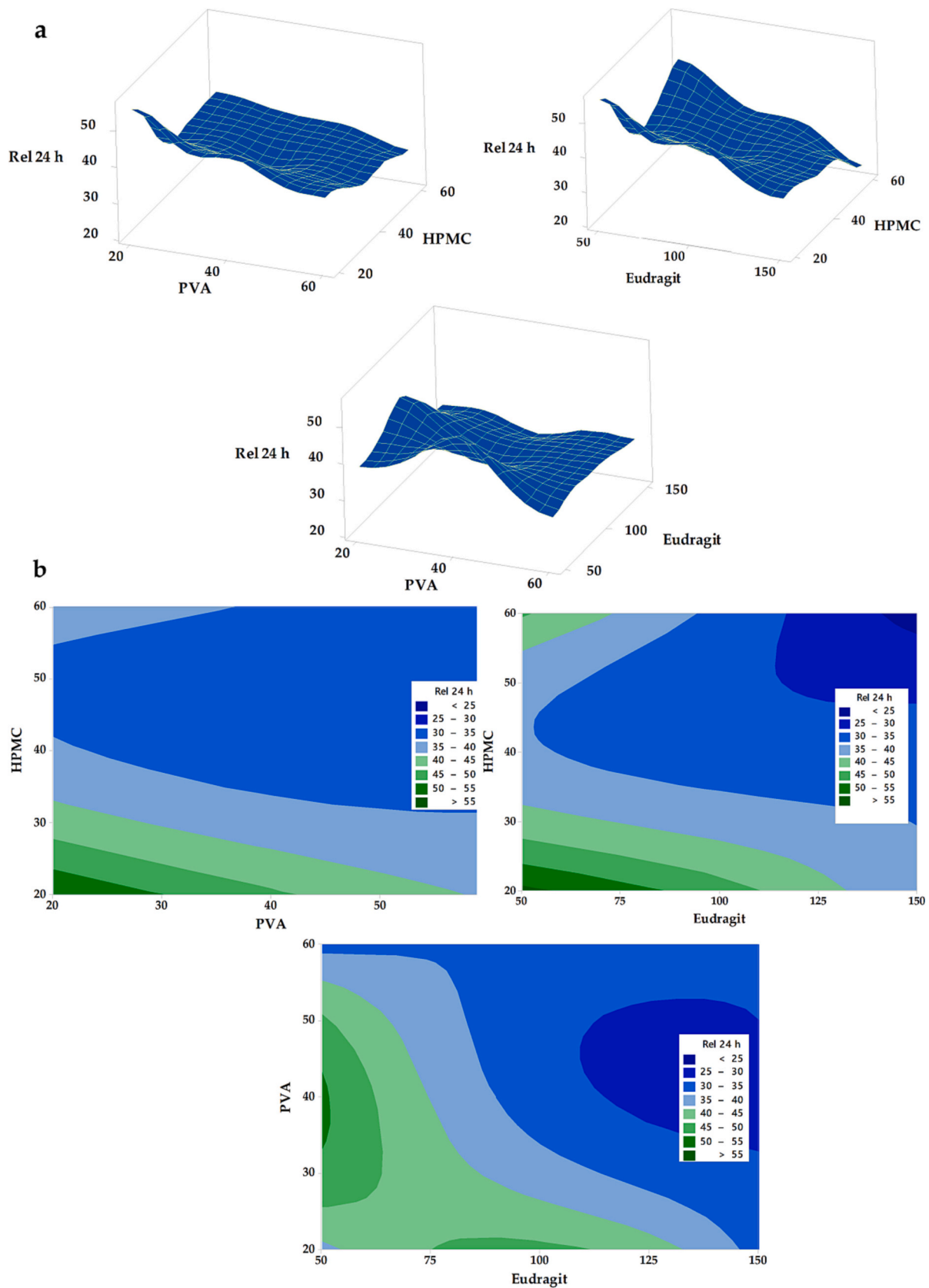
Fig. 7. (a) 3D and response surface plot for the effect of HPMC, PVA, and Eudragit RL100 (R_1, R_2, and R_3) on the cumulative VLD% released after 24 h (Z_2), (b) The contour plot for the effect of HPMC, PVA, and Eudragit RL100 (R_1, R_2, and R_3) on the cumulative VLD % released after 24 h (Z_2).
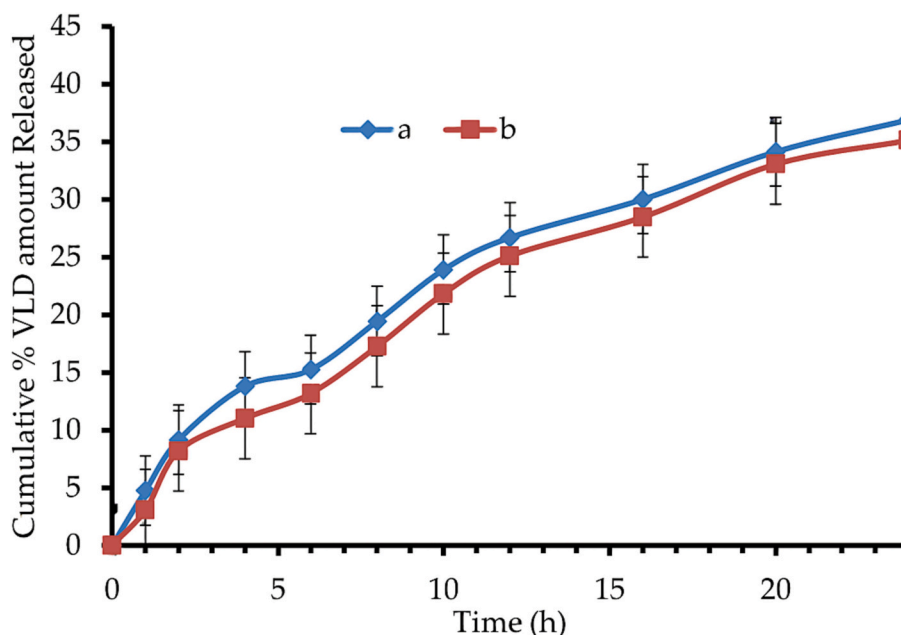
Fig. 8. Plots of a: *in vitro* and b: *in vivo*, cumulative VLD percent amount released *versus* time for the optimized VLD-SLNPs-OCUs formulation (VOS-0).

PVA, and 150 mg Eudragit RL100) were formulated and characterized for drug loading, *in vitro* release, sterility test, *in vivo* release, differential scanning calorimetry (DSC), ocular irritation test, and stability study.

3.5.1. Differential scanning calorimetry (DSC) analysis

Thermograms of differential scanning calorimetry (DSC) for pure VLD, pure components, VLD-SLNPs, and the optimized formulation (VSO-0) are shown in Fig. S11. The DSC thermogram of pure VLD showed a sharp endothermic peak at 155.7 °C, corresponding to its melting point (Dewan et al., 2015). The DSC curves of HPMC, PVA, stearic acid, and Eudragit RL100 showed endothermic peaks at 75.4, 214.2, 58.4, and 69 °C, respectively, related to the melting temperature of pure ingredients (Amin et al., 2012; Martínez-Hernández et al., 2010; Patel et al., 2021; Rani et al., 2015). The thermogram of VLD–SLNPs showed that the endothermic peak of stearic acid displaced slightly from 58.4 to 56.2 °C and the absence of the VLD endothermic peak at 155.7 °C, suggesting efficient VLD distribution within the lipid matrix and loss of its crystallinity (Yasir and Sara, 2014). The thermograms of optimized VLD-SLNPs-OCUs did not show the endothermic peak of VLD at 155.7 °C, indicating complete conversion of VLD to the amorphous state and well-distribution of VLD in the prepared OCUs matrices (El-Emam et al., 2020).

3.5.2. Sterility test

A sterility study was done for the optimized VLD-SLNPs-OCUs formulation. The result showed that there was no turbidity and no microbial growth during and after the completion of the sterility test. Also, the experiment showed no appearance of any microorganisms, thus suggesting that the prepared VLD-SLNPs-OCUs can be used safely in ophthalmic drug delivery.

3.5.3. Drug loading

Drug loading of the optimized OCUs formulation was 95.28 ± 2.78 (Table S6). The enhanced drug encapsulation in the optimized formula could be attributed to the increase in the polymer concentration (Kanaan et al., 2021).

3.5.4. In vivo release studies

The *in vivo* cumulative percent release of VLD from the optimized OCUs was 35.12 ± 2.47% after 24 h, which was consistent with the *in*

Table 6
Ocular irritation test results.

Time (day)	Observation parameters/ score			
	Redness	Increased tears production	Swelling of eyelids	Irisitis
0	0	0	0	0
1	0	1	1	0
3	0	0	0	0
5	0	0	0	0
7	0	0	0	0

vitro release data, 36.89 ± 3.11%, as shown in Fig. 8. Thus, the optimized OCU formulation may act for 24 h (once daily) (Nair et al., 2018).

3.5.5. Rabbit ocular irritation test

The data showed that no rabbits exhibited any signs of irritancy, and the total score was zero or negligible (Table 6) except for increased tear production and swelling of the eyelid after the first day of insertion, which might be due to the organic solvent (ethyl alcohol) used in the formulation of VLD-SLNPs-OCUs (Rathore et al., 2010).

3.5.6. Speeded-up stability testing

The optimized OCU formulation exhibits a nonsignificant change in the physical characteristics or drug loading (p > 0.05). The overall degradation was <1%, and the *in vitro* release profile of VLD did not alter noticeably after storage, as shown in Table S6. Thus, the optimized OCUs are sufficiently stable at the selected conditions.

4. Conclusion

The double emulsion/melt dispersion method was effectively used to create VLD-SLNPs. VLD-SLNP formulation (Run 3) was selected for incorporation into OCUs based on optimum particle size, entrapment efficiency, and *in vitro* dissolution pattern. The optimum VLD-SLNPs-OCUs were composed of 50.303 mg HPMC, 60 mg PVA, and 150 mg Eudragit RL100. VLD-SLNPs-OCUs loading efficiency was 95.28 ± 2.87%, and DSC data showed complete conversion of VLD to an amorphous state and well distribution in the prepared OCUs matrices. Consistent with *in vitro* drug release findings of 36.89 ± 3.11%, the *in*

vivo release after 24 h was 35.12 ± 2.47%. The ocular irritation test indicates the safety of using VLD-OCU fabrications. Thus, the sustained drug release provided by VLD-SLNPs-OCUs could be an effective alternative to conventional oral dosage forms with fewer systemic side effects and decreased fluctuations in plasma drug levels. Besides lowering blood sugar, VLD-OCUs may improve blood flow in the retina, making them a potentially useful method for treating DRP.

Funding

CRediT authorship contribution statement

Abd El hakim Ramadan: Conceptualization, Data curation, Formal analysis, Investigation, Methodology, Resources, Supervision, Validation, Visualization, Writing - original draft. **Mahmoud M. A. Elsayed:** Data curation, Conceptualization, Methodology, Validation, Visualization. **Amani Elsayed:** Methodology, Investigation. **Marwa A. Fouad:** Methodology, Resources, Supervision, Validation, Visualization. **Mohamed S. Mohamed:** Software, Methodology, Supervision, Validation. **Sangmin Lee:** Data curation, Formal analysis, Investigation, Methodology, Resources, Supervision. **Reda A. Mahmoud:** Software, Methodology, Supervision, Validation. **Shereen A. Sabry:** Methodology, Investigation, Resources, Supervision, Validation. **Mohammed M. Ghoneim:** Funding acquisition, Methodology, Resources, Supervision. **Ahmed H.E. Hassan:** Funding acquisition, Methodology, Writing – review & editing. **Reham A. Abd Elkarim:** Conceptualization, Data curation, Formal analysis, Investigation, Methodology, Resources, Supervision, Validation, Visualization. **Amany Belal:** Formal analysis, Investigation, Methodology, Resources. **Ahmed A. El-Shenawy:** Conceptualization, Data curation, Formal analysis, Investigation, Methodology, Supervision, Validation, Writing - original draft, Writing - review & editing.

Declaration of competing interest

The authors declare the following financial interests/personal relationships which may be considered as potential competing interests:
Amany Belal reports financial support was provided by The King Salman Center for Disability Research has supported this work through the KSRG-2023-157 Research Group. Amani Elsayed reports a relationship with The King Salman Center for Disability Research has supported this work through the KSRG-2023-157 Research Group that includes: equity or stocks and funding grants. If there are other authors, they declare that they have no known competing financial interests or personal relationships that could have appeared to influence the work reported in this paper.

Data availability

The datasets generated during and/or analyzed during the current study are available from the corresponding authors upon reasonable request.

Acknowledgments

Appendix A. Supplementary data

Supplementary data to this article can be found online at https://doi.org/10.1016/j.ijpx.2024.100232.

References

Abd Elkarim, R.A., El-Shenawy, A.A., Abdelhafez, W.A., Osman, S.K., 2022. Novel nanosized Diacerein proliposomes for oral delivery: Development and in vitro/in vivo evaluation. J. App. Pharm. Sci. 12 (7), 131–146.

Abdelhameed, A.H., Abdelhafez, W.A., Mohamed, M.S., 2022. Formulation, optimization, and in-vivo evaluation of nanostructured lipid carriers loaded with Fexofenadine HCL for oral delivery. J. Drug Deliv. Sci .Tech. 74, 103607.

Abdul Ahad, H., Sreeramulu, J., Padmaja, B.S., Reddy, M.N., Prakash, P.G., 2011. Preparation of fluconazole? - Cyclodextrin complex ocuserts: in vitro and in vivo evaluation. Int. Sch. Res. Not. 2011.

Abo-Zeid, Y., Amer, A., Bakkar, M.R., El-Houssieny, B., Sakran, W., 2022. Antimicrobial activity of Azithromycin Encapsulated into PLGA NPs: A potential strategy to overcome efflux resistance. Antibiotics 11 (11), 1623.

Aburahma, M.H., Mahmoud, A.A., 2011. Biodegradable ocular inserts for sustained delivery of brimonidine tartarate: preparation and in vitro/in vivo evaluation. AAPS PharmSciTech 12, 1335–1347.

Ahad, H.A., Chinthaginjala, H., Bhupalam, P., Dasari, R.R., Rao, B.S., Tarun, K., 2021. Designing of dexamethasone sodium phosphate ocular films for madras eye: in vitro and in vivo evaluation. Pak. J. Pharm. Sci. 34 (2).

Ahmed, M.G., 2017. Development and in vitro evaluation of rosuvastatin tablets by floating drug delivery system. Asian J. Pharm. 11 (02).

Ahmed, M.M., 2019. Effect of different formulation variables on release characteristics of gastro-floating microspheres of ethyl cellulose/carbopol 934P encapsulating sorafenib. Int J Pharm Pharm Sci 11, 64–70.

Ahmed, M.M., Abd El-Rasoul, S., Auda, S.H., Ibrahim, M.A., 2013. Emulsification/internal gelation as a method for preparation of diclofenac sodium–sodium alginate microparticles. Saudi Pharm. J. 21 (1), 61–69.

Akhter, M.H., Ahmad, I., Alshahrani, M.Y., Al-Harbi, A.I., Khalilullah, H., Afzal, O., Karim, S., 2022. Drug delivery challenges and current progress in nanocarrier-based ocular therapeutic system. Gels 8 (2), 82.

Amin, S., Mir, S., Kohli, K., Ali, A., 2012. Novel polymeric matrix films for transdermal delivery of metoclopramide. Int. J. Pharm. Fron. Res. 2 (1), 48–60.

Auda, H., Ahmed, M., El-Rasoul, A., Saleh, K., 2010. Formulation and physicochemical characterization of piroxicam containing polymer films. Bull. Pharm. Sci. Ass. 33 (1), 33–42.

Balaji, R., Duraisamy, R., Kumar, M., 2019. Complications of diabetes mellitus: A review. Drug Inv. Today 12 (1).

Baranowski, P., Karolewicz, B., Gajda, M., Pluta, J., 2014. Ophthalmic drug dosage forms: characterisation and research methods. Sci. World J. 2014.

Berndt-Zipfel, C., Michelson, G., Dworak, M., Mitry, M., Löffler, A., Pfützner, A., Forst, T., 2013. Vildagliptin in addition to metformin improves retinal blood flow and erythrocyte deformability in patients with type 2 diabetes mellitus–results from an exploratory study. Cardiovasc. Diabetol. 12, 1–7.

Boddupalli, B.M., Mohammed, Z.N., Nath, R.A., Banji, D., 2010. Mucoadhesive drug delivery system: an overview. J. Adv. Pharm. Tech. Res. 1 (4), 381.

Chauhan, I., Singh, L., 2023. A Comprehensive Literature Review of Lipids used in the Formulation of Lipid Nanoparticles. Curr. Nanomat 8 (2), 126–152.

Colter, J.M., 2016. Design Optimization of a Hyaluronic-Acid Based Hydrogel Drug-Delivery Device for Immobilization in the Eye. The University of Utah.

Costagliola, C., Agnifili, L., Arcidiacono, B., Duse, S., Fasanella, V., Mastropasqua, R., Semeraro, F., 2012. Systemic thromboembolic adverse events in patients treated with intravitreal anti-VEGF drugs for neovascular age-related macular degeneration. Exp. Opin. Bio Ther. 12 (10), 1299–1313.

Dawaba, H.M., Dawaba, A.M., 2019. Development and evaluation of extended release ciprofloxacin HCl ocular inserts employing natural and synthetic film forming agents. J. Pharm. Inv. 49, 245–257.

Dawaba, A.M., Dawaba, H.M., El-enin, A.S.A., Khalifa, M.K., 2018. Fabrication of bioadhesive ocusert with different polymers: once a day dose. Intl. J. App. Pharm. 309–317.

Dekhil, O., Naglah, A., Shaban, M., Ghazal, M., Taher, F., Elbaz, A., 2019. Deep learning based method for computer aided diagnosis of diabetic retinopathy. In: Paper Presented at the 2019 IEEE Int Conf Imag Sys Tech (IST).

Dewan, I., Islam, S., Rana, M., 2015. Characterization and compatibility studies of different rate retardant polymer loaded microspheres by solvent evaporation technique: in vitro-in vivo study of vildagliptin as a model drug. J. Drug Del. 2015.

El-Emam, G.A., Girgis, G.N., El-Sokkary, M.M.A., El-Azeem Soliman, O.A., Abd El Gawad, A.E.G.H., 2020. Ocular inserts of voriconazole-loaded proniosomal gels: formulation, evaluation and microbiological studies. Int. J. Nanomedicine 7825–7840.

Elkot, M., Elsayed, M., Alaaeldin, E., Sarhan, H., Shaykoon, M.S.A., Elsadek, B., 2019. Accelerated stability testing of microcapsulated sorafenib-loaded carbon nanotubes prepared by emulsification/internal gelation method. Int. J. Pharm. Pharm. Res. 16, 126–139.

El-Rasoul, A., Ahmed, M.M., 2010. Chitosan polymer as a coat of calcium alginate microcapsules loaded by non-steroidal antiinflammatory drug. Bull. Pharm. Sci. Ass. 33 (2), 179–186.

Elsayed, 2021. Controlled release alginate-chitosan microspheres of tolmetin sodium prepared by internal gelation technique and characterized by response surface modeling. Braz. J. Pharm. Sci. 56.

Elsayed, M.M., Mostafa, M.E., Alaaeldin, E., Sarhan, H.A., Shaykoon, M.S., Allam, S., Elsadek, B.E., 2019. Design and characterisation of novel Sorafenib-loaded carbon nanotubes with distinct tumour-suppressive activity in hepatocellular carcinoma. Int. J. Nanomedicine 14, 8445.

Elsayed, M., El Rasoul, S.A., Hussein, A.K., 2020a. Response surface methodology as a useful tool for development and optimization of sustained release ketorolac tromethamine niosomal organogels. J. Pharm. Innov. 15 (4), 664–677.

Elsayed, M.M., El Rasoul, S.A., Ramadan, A.E., Hussein, A.K., 2020b. Response surface methodology as a useful tool for development and optimization of sustained release ketorolac tromethamine niosomal organogels. J. Pharm. Innov. 15, 664–677.

Elsayed, M.M., Okda, T.M., Atwa, G.M., Omran, G.A., Abd Elbaky, A.E., Ramadan, A.E., 2021. Design and optimization of orally administered luteolin nanoethosomes to enhance its anti-tumor activity against hepatocellular carcinoma. Pharmaceutics 13 (5), 648.

Elsayed, M.M., Aboelez, M.O., Elsadek, B.E., Sarhan, H.A., Khaled, K.A., Belal, A., Elkaeed, E.B., 2022a. Tolmetin sodium fast dissolving tablets for rheumatoid arthritis treatment: preparation and optimization using Box-Behnken design and response surface methodology. Pharmaceutics 14 (4), 880.

Elsayed, M.M., Aboelez, M.O., Mohamed, M.S., Mahmoud, R.A., El-Shenawy, A.A., Mahmoud, E.A., Elsadek, M.E.M., 2022b. Tailoring of rosuvastatin calcium and atenolol bilayer tablets for the management of hyperlipidemia associated with hypertension: A preclinical study. Pharmaceutics 14 (8), 1629.

El-Shenawy, A.A., Abdelhafez, W.A., Ismail, A., Kassem, A.A., 2020. Formulation and characterization of nanosized ethosomal formulations of antigout model drug (febuxostat) prepared by cold method: in vitro/ex vivo and in vivo assessment. AAPS PharmSciTech 21, 1–13.

El-Shenawy, A.A., Mahmoud, R.A., Mahmoud, E.A., Mohamed, M.S., 2021. Intranasal in Situ Gel of Apixaban-Loaded Nanoethosomes: Preparation, Optimization, and in Vivo Evaluation. AAPS PharmSciTech 22 (4), 147.

El-Shenawy, A.A., Elsayed, M.M., Atwa, G.M., Abourehab, M.A., Mohamed, M.S., Ghoneim, M.M., El-Sherbiny, M., 2023. Anti-Tumor activity of Orally Administered Gefitinib-Loaded Nanosized Cubosomes against Colon Cancer. Pharmaceutics 15 (2), 680.

Emami, J., Mohiti, H., Hamishehkar, H., Varshosaz, J., 2015. Formulation and optimization of solid lipid nanoparticle formulation for pulmonary delivery of budesonide using Taguchi and Box-Behnken design. Res. Pharm. Sci. 10 (1), 17.

Gao, C., Yu, S., Zhang, X., Dang, Y., Han, D.-D., Liu, X., Hui, M., 2021. Dual functional Eudragit® S100/L30D-55 and PLGA colon-targeted nanoparticles of iridoid glycoside for improved treatment of induced ulcerative colitis. Int. J. Nanomedicine 16, 1405.

Garrison, K.L., Sahin, S., Benet, L.Z., 2015. Few drugs display flip-flop pharmacokinetics and these are primarily associated with classes 3 and 4 of the BDDCS. J. Pharm. Sci. 104 (9), 3229–3235.

Hasan, A., Abd El Hakim Ramadan, M.A., Elghany, S.S., 2020. Design and characterization of intra-oral fast dissolving tablets containing diacerein-solid dispersion. J. App. Pharm. Sci. 10 (06), 044–053.

Hesham, M., Jelan, A., Mahmoud, A., 2015. Development and optimization of itopride hydrochloride fast disintegrating tablets using factorial design and response surface methodology. Int. J. Pharm. Sci. Res. 6 (4), 1661–1672.

Hind, H.W., Goyan, F.M., 1949. The hydrogen ion concentration and osmotic properties of lacrimal fluid. J. Am. Pharm. Ass. 38 (9), 477–479.

Iqbal, F.M., Ahmad, M., Tulain, U.R., 2017. Microwave radiation induced synthesis of hydroxypropyl methylcellulose-graft-(polyvinylalcohal-co-acrylic acid) polymeric network and its in vitro evaluation. Acta Pol. Pharm. Drug Res. 74, 527–541.

Jampilek, J., Kralova, K., 2020. Potential of nanonutraceuticals in increasing immunity. Nanomaterials 10 (11), 2224.

Kanaan, M.Q., Numan, N.A., Shakya, A.K., Tawfiq, F.A., 2021. Formulation and release of timolol maleate from ocusert based on gelatin-N-(3-dimethylaminopropyl)-N-ethylcarbodiimide polymer. J. Pharm. Pharm. Res. 9 (2), 182–194.

Kerkhof, H.J., Bierma-Zeinstra, S.M., Castano-Betancourt, M.C., de Maat, M.P., Hofman, A., Pols, H.A., van Meurs, J.B., 2010. Serum C reactive protein levels and genetic variation in the CRP gene are not associated with the prevalence, incidence or progression of osteoarthritis independent of body mass index. Ann. Rheum. Dis. annrheumdis. 125260 69 (11), 1976–1982.

Kodavaty, J., Deshpande, A.P., 2014. Mechanical and swelling properties of poly (vinyl alcohol) and hyaluronic acid gels used in biomaterial systems - a comparative study. Def. Sci. J. 64 (3).

Kulhari, H., Pooja, D., Narayan, H., Meena, L., Prajapati, S., 2011. Design and evaluation of ocusert for controlled delivery of flurbiprofen sodium. Curr. Eye Res. 36 (5), 436–441.

Langevin, D., Poteau, S., Hénaut, I., Argillier, J., 2004. Crude oil emulsion properties and their application to heavy oil transportation. Oil Gas Sci. Technol. 59 (5), 511–521.

Leske, M.C., Wu, S.-Y., Hennis, A., Hyman, L., Nemesure, B., Yang, L., Group, B.E.S., 2005. Hyperglycemia, blood pressure, and the 9-year incidence of diabetic retinopathy: the Barbados Eye Studies. Ophthalmology 112 (5), 799–805.

Manjunath, K., Reddy, J.S., Venkateswarlu, V., 2005. Solid lipid nanoparticles as drug delivery systems. Methods Find. Exp. Clin. Pharmacol. 27 (2), 127–144.

Mansour, S.E., Browning, D.J., Wong, K., Flynn Jr., H.W., Bhavsar, A.R., 2020. The evolving treatment of diabetic retinopathy. Clin. Ophthalmol. 653–678.

Martínez-Hernández, A.L., Velasco-Santos, C., Castano, V., 2010. Carbon nanotubes composites: processing, grafting and mechanical and thermal properties. Curr. Nanosci. 6 (1), 12–39.

Mbata, O., El-Magd, N.F.A., El-Remessy, A.B., 2017. Obesity, metabolic syndrome and diabetic retinopathy: beyond hyperglycemia. World J. Diabetes 8 (7), 317.

Mehrad, B., Ravanfar, R., Licker, J., Regenstein, J.M., Abbaspourrad, A., 2018. Enhancing the physicochemical stability of β-carotene solid lipid nanoparticle (SLNP) using whey protein isolate. Food Res. Int. 105, 962–969.

Mohamed, M.S., Abdelhafez, W.A., Zayed, G., Samy, A.M., 2019. In vitro and in vivo characterization of fast dissolving tablets containing gliquidone–pluronic solid dispersion. Drug Dev. Ind. Pharm. 45 (12), 1973–1981.

Nagpal, M.A., Sharma, K., Anand, N., Singh, D., Dhawan, R., Usman, M.R.M., Nagpal, N., 2020. Preparation and evaluation of sulfacetamide sodium ocusert for controlled drug delivery. J. Drug Deliv. Ther. 10 (2), 164–170.

Naguib, M.J., Hassan, Y.R., Abd-Elsalam, W.H., 2021. 3D printed ocusert laden with ultra-fluidic glycerosomes of ganciclovir for the management of ocular cytomegalovirus retinitis. Int. J. Pharm. 607, 121010.

Nair, R.V., Shefrin, S., Suresh, A., Anoop, K., Nair, S.C., 2018. Sustained release timolol maleate loaded ocusert based on biopolymer composite. Int. J. Biol. Macromol. 110, 308–317.

Nandi, S., Ojha, A., Nanda, A., Sahoo, R.N., Swain, R., Pattnaik, K.P., Mallick, S., 2022. Vildagliptin plasticized hydrogel film in the control of ocular inflammation after topical application: study of hydration and erosion behaviour. Z. Phys. Chem. 236 (2), 275–290.

Nithiyananthan, T., Shankarananth, V., Rajasekhar, K., Jyothikrishna, K., Mukesh, O., Vikram, K., 2009. Preparation and evaluation of ciprofloxacin ocuserts. J. Pharm. Res. 2 (9), 1496–1499.

Patel, D.K., Kesharwani, R., Kumar, V., 2021. Nanostructured Lipid carrier (NLC) and Solid Lipid Nanoparticles (SLN) based Hydrogel for delivery of Etodolac: A Comparative Investigation on Dermal Pharmacokinetic on Rat Skin. Int. J. Pharm. Inves. 11 (2).

Paul, S., Pathak, H., Sharma, H.K., 2022. An overview on nanocarriers. Nanocarr. Drug Targ. Brain Tum. 145–204.

Peres, L.B., Peres, L.B., de Araújo, P.H.H., Sayer, C., 2016. Solid lipid nanoparticles for encapsulation of hydrophilic drugs by an organic solvent free double emulsion technique. Colloids Surf. B: Biointerfaces 140, 317–323.

Permana, A.D., Tekko, I.A., McCrudden, M.T., Anjani, Q.K., Ramadon, D., McCarthy, H.O., Donnelly, R.F., 2019. Solid lipid nanoparticle-based dissolving microneedles: A promising intradermal lymph targeting drug delivery system with potential for enhanced treatment of lymphatic filariasis. J. Control. Release 316, 34–52.

Porta, M., Bandello, F., 2002. Diabetic retinopathy: a clinical update. Diabetologia 45, 1617–1634.

Rahić, O., Tucak, A., Omerović, N., Sirbubalo, M., Hindija, L., Hadžiabdić, J., Vranić, E., 2020. Novel drug delivery systems fighting glaucoma: Formulation obstacles and solutions. Pharmaceutics 13 (1), 28.

Ramkanth, S., Chetty, C.M., Alagusundaram, M., Angalaparameswari, S., Thiruvengadarajan, V., Gnanaprakash, K., 2009. Design and evaluation of diclofenac sodium ocusert. Int. J. Pharm. Tech. Res. 1 (4), 1219–1223.

Rampino, A., Borgogna, M., Blasi, P., Bellich, B., Cesàro, A., 2013. Chitosan nanoparticles: Preparation, size evolution and stability. Int. J. Pharm. 455 (1–2), 219–228.

Rani, N.S., Sannappa, J., Demappa, T., 2015. Effects of CdCl 2 concentration on the structural, thermal and ionic conductivity properties of HPMC polymer electrolyte films. Ionics 21, 133–140.

Rao, S.V., Tejaswi, B., Anusha, A., Padmalatha, K., 2018. Fluconazole Ocuserts: Formulation and Evaluation. J. Pharm. Sci. Res. 10 (1), 26–30.

Rathod, L.V., Kapadia, R., Sawant, K.K., 2017. A novel nanoparticles impregnated ocular insert for enhanced bioavailability to posterior segment of eye: in vitro, in vivo and stability studies. Mater. Sci. Eng. C 71, 529–540.

Rathore, K.S., Nema, R.K., Sisodia, S.S., 2010. Timolol maleate a gold standard drug in glaucoma used as ocular films and inserts: an overview. Int. J. Pharm. Sci. Rev. Res. 3 (1), 23–29.

Reddy, E.S., 2017. Design and characterization of ofloxacin and dexamethasone ocular inserts using combination of hydrophobic and hydrophilic polymers. Asian J. Pharm. 11 (01).

Refaat, H., Naguib, Y.W., Elsayed, M., Sarhan, H.A., Alaaeldin, E., 2019. Modified spraying technique and response surface methodology for the preparation and optimization of propolis liposomes of enhanced anti-proliferative activity against human melanoma cell line A375. Pharmaceutics 11 (11), 558.

Repka, M.X., Tung, B., Good, W.V., Shapiro, M., Capone, A., Baker, J.D., van Heuven, W., 2006. Outcome of eyes developing retinal detachment during the early Treatment for Retinopathy of Prematurity Study (ETROP). Arch. Ophthalmol. 124 (1), 24–30.

Roy Choudhury, S., Mandal, A., Chakravorty, D., Gopal, M., Goswami, A., 2013. Evaluation of physicochemical properties, and antimicrobial efficacy of monoclinic sulfur-nanocolloid. J. Nanopart. Res. 15, 1–11.

Sabry, S., Okda, T., Hasan, A., 2021. Formulation, characterization, and evaluation of the anti-tumor activity of nanosized galangin loaded niosomes on chemically induced hepatocellular carcinoma in rats. J. Drug Deliv. Sci .Tech. 61, 102163.

Sahoo, S.K., Dilnawaz, F., Krishnakumar, S., 2008. Nanotechnology in ocular drug delivery. Drug Discov. Today 13 (3–4), 144–151.

Senthil Kumar, K., Ashok, K., Dhachinamoorth, D., Sudhakar, Y., 2017. Formulation and evaluation of controlled release ocuserts of levofloxacin hydrochloride. Int. J. Innov. Pharm. Sci. Res. 5 (1), 13–26.

Seyfoddin, A., Shaw, J., Al-Kassas, R., 2010. Solid lipid nanoparticles for ocular drug delivery. Drug Deliv. 17 (7), 467–489.

Shafie, M.A.A., Rady, M.A.H., 2012. In vitro and in vivo evaluation of timolol maleate ocular inserts using different polymers. J. Clin. Exp. Ophthalmol. 3, 246.

Shanmugam, S., Valarmathi, S., Kumar, S.S., Shanmugasundaram, P., Senthilkumar, M., 2016. Formulation development and evaluation of opthalmic ocusert containing aciclovir. Res. J. Pharm. Tech. 9 (11), 1858–1862.

Sharma, M., Sharma, V., Panda, A.K., Majumdar, D.K., 2011. Development of enteric submicron particle formulation of papain for oral delivery. Int. J. Nanomedicine 2097–2111.

Shivhare, R., Pathak, A., Shrivastava, N., Singh, C., Tiwari, G., Goyal, R., 2012. An update review on novel advanced ocular drug delivery system. World J. Pharm. Pharm. Sci. 1 (2), 545–568.

Shrestha, P., Bhandari, S.K., Islam, S., Reza, M.S., Adhikari, S., 2014. Design and development of immediate and sustained release tablets of vildagliptin. Res. J. Pharm., Biol. Chem. Sci. 5, 811.

Solanki, A.B., Parikh, J.R., Parikh, R.H., 2007. Formulation and optimization of piroxicam proniosomes by 3-factor, 3-level Box-Behnken design. AAPS PharmSciTech 8, 43–49.

Spoorthy, M., Ramesh, K., Kumar, G., 2023. Development and evaluation of lovastatin transdermal delivery system using polymeric and solid lipid nanoparticles. J. Pharm. Neg. Res. 1391–1400.

Stewart, M.W., 2012. Corticosteroid use for diabetic macular edema: old fad or new trend? Curr. Diab. Rep. 12, 364–375.

Subedi, R.K., Kang, K.W., Choi, H.-K., 2009. Preparation and characterization of solid lipid nanoparticles loaded with doxorubicin. Eur. J. Pharm. Sci. 37 (3–4), 508–513.

Takeuchi, Y., Ikeda, N., Tahara, K., Takeuchi, H., 2020. Mechanical characteristics of orally disintegrating films: Comparison of folding endurance and tensile properties. Int. J. Pharm. 589, 119876.

Thakur, R., Swami, G., Rahman, M., 2014. Development and optimization of controlled release bioerodable anti infective ophthalmic insert. Curr. Drug Deliv. 11 (1), 2–10.

Tofighia, P., Soltani, S., Montazam, S.H., Montazam, S.A., Jelvehgari, M., 2017. Formulation of tolmetin ocuserts as carriers for ocular drug delivery system. IJPR 16 (2), 432.

Wu, Y.-J., Guo, X., Li, C.-J., Li, D.-Q., Zhang, J., Yang, Y., Chen, L.-M., 2015. Dipeptidyl peptidase-4 inhibitor, vildagliptin, inhibits pancreatic beta cell apoptosis in association with its effects suppressing endoplasmic reticulum stress in db/db mice. Metabolism 64 (2), 226–235.

Yasir, M., Sara, U.V.S., 2014. Solid lipid nanoparticles for nose to brain delivery of haloperidol: in vitro drug release and pharmacokinetics evaluation. Acta Pharm. Sin. B 4 (6), 454–463.

Zhu, J., Liu, B., Li, L., Zeng, Z., Zhao, W., Wang, G., Guan, X., 2016. Simple and green fabrication of a superhydrophobic surface by one-step immersion for continuous oil/water separation. J. Phys. Chem. A 120 (28), 5617–5623.